NASA TN D-1527

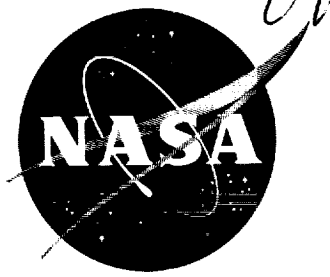

TECHNICAL NOTE

D-1527

HEAT TRANSFER IN LAMINAR FLOWS OF INCOMPRESSIBLE FLUIDS WITH $Pr \to 0$ AND $Pr \to \infty$

By Ernst W. Adams

George C. Marshall Space Flight Center
Huntsville, Alabama

NATIONAL AERONAUTICS AND SPACE ADMINISTRATION
WASHINGTON
February 1963

Copy 1

Code 1

NATIONAL AERONAUTICS AND SPACE ADMINISTRATION

TECHNICAL NOTE D-1527

HEAT TRANSFER IN LAMINAR FLOWS OF INCOMPRESSIBLE FLUIDS WITH $Pr \to 0$ AND $Pr \to \infty$

By Ernst W. Adams

SUMMARY

Exact closed form solutions of the boundary layer equations can be derived for the Nusselt number Nu(x) at the leading edge x = 0 and, in the limits $Pr \to 0$ and $Pr \to \infty$, on the surface $x \geq 0$ of arbitrary bodies in planar uniform flow. Exact and approximate solutions for Nu(x)/Nu(0) in the range $0 < Pr < \infty$ are compared to the results of the $Pr \to 0$ and the $Pr \to \infty$ methods. It is shown theoretically and confirmed by the numerical results that the $Pr \to 0$ method yields an upper limit for Nu(x)/Nu(0). The presented examples show that the $Pr \to \infty$ method yields a lower limit for Nu(x)/Nu(0) in case of slender bodies. In the cases for which similarity solutions exist, both methods yield the exact solution for Nu(x)/Nu(x*) where x* is any reference station. By use of exact stagnation point solutions for $Nu(0)/\sqrt{Re}$, the $Pr \to 0$ and the $Pr \to \infty$ methods may be applied to obtain engineering estimates of the heat transfer parameter $Nu(x)/\sqrt{Re}$.

I. INTRODUCTION

Many engineering problems involve the case treated in this paper, the heat exchange between an impermeable wall and the planar laminar flow of an incompressible fluid with constant material properties under the assumption of negligible frictional heating. The mathematical treatment of this problem starts from the equations of continuity, momentum, and energy. The boundary layer versions of the equations of momentum and energy may be employed if both the Reynolds number $Re = L\rho u_\infty/\mu$ and the Peclet number Pe = Re Pr are sufficiently large, where $Pr = \mu g c_p/k$ is the Prandtl number. Exact solutions of this boundary layer problem are presented in references 2, 5, 8, 10, 13, 16, and 22. Integral solutions of the Karman-Pohlhausen type are presented in references 4, 17, and 23. The energy equation for the temperature distribution in the boundary layer is a linear second-order differential

equation, which can be integrated analytically only in special cases because of the explicit occurrence of the velocity components $u(x,y)$ and $v(x,y)$ as coefficients in this equation.

The integration becomes generally feasible in the limiting cases $Pr \to 0$ and $Pr \to \infty$. If δ_v is the thickness of the velocity boundary layer and if δ_t is the thickness of the temperature boundary layer, $\lim_{Pr \to 0}\left(\frac{\delta_v}{\delta_t}\right) = 0$ and $\lim_{Pr \to \infty}\left(\frac{\delta_t}{\delta_v}\right) = 0$. The process $Pr \to 0$ is compatible with the above mentioned condition $Pe = Re\ Pr = (u_\infty L)(\rho\ g\ c_p/k) \gg 1$ if it is accomplished by $\mu \to 0$. For $Pr \to 0$, then the velocity distribution $u(x,y)$ throughout the temperature boundary layer may be approximated by the velocity distribution $u_e(x)$ at the outer edge of the boundary layer; $u_e(x)$ is a result of ideal fluid theory and, correspondingly, violates the no-slip condition, $u(x,0) = 0$, at the wall. For $Pr \to \infty$, the velocity distribution $u(x,y)$ throughout the temperature boundary layer may be approximated by the wall tangent $u = y\ \tau_w(x)/\mu$, where τ_w is the wall shear stress.

Lighthill presented an exact analysis for the approach $Pr \to \infty$ in reference 12. References 3, 11, and 20 treat approximately valid extensions of Lighthill's "High Prandtl Number Method," $Pr \to \infty$, by the inclusion of a quadratic term in the expression for $u(x,y)$. It seems that the application of the approach $Pr \to 0$ first appeared on pp. 597-600 of reference 7. Reference 14 presents the basic equations for the "Low Prandtl Number Method," $Pr \to 0$, and the equations for a first-order correction as part of a series expansion in terms of powers of Pr. The rather involved correction terms are worked out in reference 14 only for power laws representing the speed $u_e(x)$ at the outer edge of the boundary layer and the wall temperature $T_w(x)$. Fig. 1, which is taken from reference 14, shows for constant wall temperature and zero pressure gradient that the first-order correction improves the results of the approach $Pr \to 0$ only for $Pr < 0.1$.

This paper presents a comparative evaluation of the high and the low Prandtl number methods and of published exact or approximate solutions for the range $0 < Pr < \infty$.

DEFINITION OF SYMBOLS

$c = \frac{L}{x}\frac{ue(x)}{u_\infty}$	Velocity gradient at stagnation point
$c_f = \frac{2\tau_w(x)}{\rho u_\infty^2}$	Wall friction coefficient
c_p = kcal/kg °K	Specific heat
C	Constant in the equation (19)
g m/sec^2	Gravity constant
k kcal/m °K sec	Thermal conductivity
L m	Reference length
m and n	Exponents in the equation (19)
$Nu_1 = \frac{Lq_w(x)}{k[T_w(0)-T_o]}$	Nusselt number defined in the equation (15)
$Nu_2 = \frac{xq_w(x)}{k[T_w(x)-T_o]}$	Nusselt number defined in the equation (20)
$Pr = \frac{\mu g\ c_p}{k}$	Prandtl number
p kg/m^2	Pressure
$q_w = -k\frac{\partial T(x,0)}{\partial y}$ kcal/m^{2}sec	Wall heat transfer
$Re_1 = \frac{L\rho\ u_\infty}{\mu}$	Reynolds number defined in the equation (13)
$Re_2 = \frac{x\rho\ u_e(x)}{\mu}$	Reynolds number defined in the equation (20)
T °K	Temperature
T_o °K	Constant temperature at outer edge of boundary layer

DEFINITION OF SYMBOLS (Cont'd)

T_w	°K	Wall temperature
u	m/sec	Velocity component in x-direction
u_e	m/sec	Velocity at outer edge of boundary layer
u_∞	m/sec	Speed of ambient uniform flow
v	m/sec	Velocity component in y-direction
x	m	Coordinate measuring parallel to wall
x^*	m	Reference value on x-scale
y	m	Coordinate measuring normal to wall
δ_t	m	Thickness of thermal boundary layer
δ_v	m	Thickness of velocity boundary layer
ϕ		Angle, Fig. 5
$\varnothing = \int_0^x u_e(x)dx$	m^2/sec	Velocity potential
ψ	m^2/sec	Stream Function
ρ	kg sec^2/m^4	Density
μ	kg sec/m^2	Viscosity
ξ	m	Dummy variable for x
η	m^2/sec	Dummy variable for $\varnothing$
τ_w	$\frac{kg}{m^2}$	Wall shear stress

ACKNOWLEDGEMENT

The author wishes to acknowledge the very concientious assistance of Mr. C. Lee Fox in preparing the material presented in this paper.

II. THE LOW PRANDTL NUMBER METHOD

The boundary layer problem under consideration is governed by the three differential equations

$$\frac{\partial u}{\partial x} + \frac{\partial v}{\partial y} = 0, \text{ continuity equation,} \tag{1}$$

$$u \frac{\partial u}{\partial x} + v \frac{\partial u}{\partial y} = - \frac{1}{\rho} \frac{dp}{dx} + \frac{\mu}{\rho} \frac{\partial^2 u}{\partial y^2}, \quad \text{momentum equation, and} \tag{2}$$

$$u \frac{\partial T}{\partial x} + v \frac{\partial T}{\partial y} = \frac{k}{\rho g \, c_p} \frac{\partial^2 T}{\partial y^2}, \quad \text{energy equation,} \tag{3}$$

(see, e.g., p. 136/37 of reference 15). The continuity equation (1) can be satisfied by a stream function ψ so that

$$\frac{\partial \psi(x,y)}{\partial y} = u(x,y) \quad \text{and} \quad \frac{\partial \psi(x,y)}{\partial x} = -v(x,y). \tag{4}$$

The von Mises transformation is introduced in order to replace x and y by x and $\psi(x,y)$ in the energy equation (3). If the derivative with respect to x when y is constant is denoted by $(\partial/\partial x)_y$, with a similar notation for other derivatives, the following transformation formulae may be derived (see p. 152 of reference 15):

$$\left(\frac{\partial}{\partial x}\right)_y = \left(\frac{\partial}{\partial x}\right)_\psi + \left(\frac{\partial}{\partial \psi}\right)_x \left(\frac{\partial \psi}{\partial x}\right)_y = \left(\frac{\partial}{\partial x}\right)_\psi - v \left(\frac{\partial}{\partial \psi}\right)_x \quad \text{and}$$

$$\left(\frac{\partial}{\partial y}\right)_x = \left(\frac{\partial}{\partial \psi}\right)_x \left(\frac{\partial \psi}{\partial y}\right)_x = u \left(\frac{\partial}{\partial \psi}\right)_x \tag{5}$$

The relations (3) and (5) yield the equation

$$\frac{\partial T}{\partial x} = \frac{k}{\rho g \, c_p} \frac{\partial}{\partial \psi} \left[u \frac{\partial T}{\partial \psi} \right]. \tag{6}$$

As $Pr \to 0$ through $\mu \to 0$, the energy equation (6) may be replaced by

$$\frac{\partial T}{\partial \varnothing} = \frac{k}{\rho g \, c_p} \frac{\partial^2 T}{\partial \psi^2}, \tag{7}$$

where $\emptyset(x) = \int_0^x u_e(x)dx$. The following initial and boundary conditions are assumed for the solution of the energy equation (7):

$$T(0, \psi) = T_o = \text{const.}, \text{ for } \psi > 0, \text{ at the leading edge } \emptyset = x = 0, \tag{8}$$

$$T(\emptyset, 0) = T_w(\emptyset), \text{ for } \emptyset \geq 0, \text{ at the wall } \psi = 0, \text{ where } T_w(0) \neq T_o \tag{9}$$

in general, and

$$\lim_{\psi \to \infty} T(\emptyset, \psi) = T_o = \text{const.} \quad \text{at the outer edge of the boundary layer} \tag{10}$$

where $T_w(\emptyset)$ is a given continuously differentiable function of $\emptyset$.

Equations (7) through (10) determine a problem of the type of transient one-dimensional heat conduction. The application of pertinent solution methods in reference 1 yields the equation (A-13) in the appendix

$$q_w(x) = \sqrt{\frac{k\rho g\, c_p}{\pi}}\, u_e(x)\left[\frac{T_w(0)-T_o}{\sqrt{\emptyset(x)}} + \int_{\eta=0}^{\eta=\emptyset(x)} \frac{dT_w(\eta)}{d\eta}\, \frac{d\eta}{\sqrt{\emptyset(x)-\eta}}\right] \tag{11}$$

for the heat transfer rate $q_w(x) = -k\partial T(x,0)/\partial y$ at the wall $y = 0$. Since $d\emptyset(x)/dx = u_e(x) > 0$ between the forward stagnation point $x = 0$ and the trailing edge, equation (11) may be replaced by

$$q_w(x) = \sqrt{\pi^{-1}\left(\frac{\mu g c_p}{k}\right)\left(\frac{L\rho u_\infty}{\mu}\right)}\, \frac{k}{L}\left[T_w(0)-T_o\right] \frac{u_e(x)}{u_\infty}\left[\frac{1}{\sqrt{\frac{\emptyset(x)}{u_\infty L}}} + \right.$$

$$\left. + \int_{\xi=0}^{\xi=x} \frac{d}{d\frac{\xi}{L}}\left(\frac{T_w(\xi)-T_o}{T_w(0)-T_o}\right) \frac{d\frac{\xi}{L}}{\sqrt{\frac{\emptyset(x)-\emptyset(\xi)}{u_\infty L}}}\right]. \tag{12}$$

The following definitions of the Reynolds number, Prandtl number, and Nusselt number are employed:

$$Re_1 = \frac{L\rho u_\infty}{\mu}, \tag{13}$$

$$Pr = \frac{\mu g c_p}{k}, \quad \text{and} \tag{14}$$

$$Nu_1(x) = \frac{L\, q_w(x)}{k[T_w(0)-T_o]}\,. \tag{15}$$

According to p. 70, reference 19,

$$\frac{u_e(x)}{u_\infty} = c\,\frac{x}{L} \qquad \text{with } c = \text{const.} \tag{16}$$

in a small vicinity of the forward stagnation point, i.e.,

$$\lim_{x\to 0} \frac{u_e(x)/u_\infty}{\sqrt{\phi(x)/u_\infty L}} = \sqrt{2c} \quad \text{and} \quad Nu_1(0) = \sqrt{Re_1\, Pr\, \frac{2c}{\pi}}. \tag{17}$$

Thus the following relation may be derived for $x \geq 0$:

$$\frac{Nu_1(x)}{Nu_1(0)} = \frac{1}{\sqrt{2c}}\left[\frac{\frac{u_e(x)}{u_\infty}}{\sqrt{\frac{\phi(x)}{u_\infty L}}} + \frac{u_e(x)}{u_\infty}\int_{\xi=0}^{\xi=x} \frac{d}{d\,\frac{\xi}{L}}\left(\frac{T_w(\xi)-T_o}{T_w(0)-T_o}\right)\frac{d\,\frac{\xi}{L}}{\sqrt{\frac{\phi(x)-\phi(\xi)}{u_\infty L}}}\right]. \tag{18}$$

III. APPLICATION OF THE LOW PRANDTL NUMBER METHOD TO CASES FOR WHICH SIMILARITY SOLUTIONS EXIST

Similarity solutions of the boundary layer equations (1) through (3) exist if the material properties are constant and if the power laws

$$\frac{u_e(x)}{u_\infty} = C\left(\frac{x}{L}\right)^m \quad \text{and} \quad T_w(x)-T_o = \begin{cases} T_o D\left(\frac{x}{L}\right)^n & \text{for } n \neq 0, \text{ or} \\ T_w(0)-T_o = \text{const}, \end{cases} \tag{19}$$

are valid, where C, D, m, and n are constant numbers. For convenience, the Reynolds number and the Nusselt number are defined here as follows:

$$Re_2(x) = \frac{\rho x\, u_e(x)}{\mu} \quad \text{and} \quad Nu_2(x) = \frac{x q_w(x)}{k[T_w(x)-T_o]}. \tag{20}$$

Data for $Nu_2(x)/\sqrt{Re_2(x)}$ resulting from exact numerical similarity solutions of the equations (1) through (3) are derived in references 5 and 10 for several sets of values m, n, and Pr. Reference 12 presents additional results for n = 0 and Pr = 0.7. The data presented in reference 10, which pertains to the ranges $-0.0904 \leq m \leq 4$, $-2.5 \leq n \leq 4$, and $0.7 \leq Pr \leq 20$ may be correlated with a ± 5% margin of error by the function

$$\frac{Nu_2(x)}{\sqrt{Re_2(x)}} = Pr^{\lambda(m)} B_o(m,n), \tag{21}$$

where

$$B_o(m,n) = 0.57\ (0.205+\beta)^{0.104} \sqrt{\frac{m+1}{2}} \left(1+\beta\,\frac{n}{m}\right)^{0.37+0.06\beta}, \tag{22}$$

$0.254 \leq \lambda(m) \leq 0.367$, and $\beta = 2m/(m+1)$.

Since, according to equation (19),

$$\phi(x) = \int_o^x u_e(x)dx = \frac{u_\infty CL}{m+1}\left(\frac{x}{L}\right)^{m+1}, \tag{23}$$

$$q_w(x) = \frac{k}{x}\left[T_w(0)-T_o\right] \sqrt{\frac{m+1}{\pi}}\ \sqrt{Pr\ Re_2(x)} \tag{24}$$

for <u>constant wall temperature</u>. The heat transfer parameter then takes the following form:

$$\frac{Nu_2(x)}{\sqrt{Re_2(x)}} \equiv \frac{x q_w(x)}{k[T_w(0)-T_o]\sqrt{Re_2(x)}} = \sqrt{Pr\ \frac{m+1}{\pi}}. \tag{25}$$

Equation (11) becomes in case of the power laws (19) for $u_e(x)$ and $T_w(x)-T_o$, i.e., in case of <u>variable wall temperature</u>,

$$q_w(x) = k\sqrt{\frac{PrRe_2(x)}{\pi}}\sqrt{\frac{u_e(x)}{x}}\frac{T_w(x)-T_o}{\left(\frac{x}{L}\right)^n}\left(\frac{m+1}{u_\infty CL}\right)^{\frac{n}{m+1}} \int_{\eta=0}^{\eta=\phi(x)} \frac{d}{d\eta}(\eta)^{\frac{n}{m+1}} \frac{d\eta}{\sqrt{\phi(x)-\eta}} \tag{26}$$

The heat transfer parameter then takes the form

$$\frac{Nu_2(x)}{\sqrt{Re_2(x)}} = \sqrt{\frac{u_\infty CL}{\pi}}\ \sqrt{Pr}\ \frac{n}{m+1}\left(\frac{m+1}{u_\infty CL}\right)^{\frac{n}{m+1}}\left(\frac{x}{L}\right)^{\frac{m+1}{2}-n} J_1(x), \tag{27}$$

where

$$J_1(x) = \phi(x)^M \int_{\frac{\eta}{\phi}=0}^{\frac{\eta}{\phi}=1} \frac{\left(\frac{\eta}{\phi}\right)^M d\left(\frac{\eta}{\phi}\right)}{\sqrt{\left(1-\frac{\eta}{\phi}\right)\frac{\eta}{\phi}}} \quad \text{and} \quad M = \frac{n}{m+1} - \frac{1}{2}\,. \tag{28}$$

The right-hand side of equation (27) is independent of x because of the relations (23) and (28); therefore,

$$\frac{Nu_2(x)}{\sqrt{Re_2(x)}} = Pr^{1/2}\ B_1(m,n). \tag{29}$$

The function J_1 can be evaluated in closed form when M is a positive integer number, and the following values may be obtained for $B_1(m,n)$ in case of suitably selected pairs of numbers m and n:

m	0	0.25	1	1	4
n	0.5	1.875	1	3	2.5
$B_1(m,n)$	0.8862	1.4862	1.2533	1.8800	1.9817

IV. THE HIGH PRANDTL NUMBER METHOD

Lighthill approximates the velocity profile u(x,y) in the limit $Pr \to \infty$ by the expression

$$u(x,y) = \frac{\tau_w(x)}{\mu}\, y = \sqrt{\frac{2\tau_w(x)}{\mu}}\ \sqrt{\psi(x,y)}, \tag{30}$$

where $\psi(x,y) = \int_0^y u(x,y)dx = y^2\tau_w(x)/2\mu$. The substitute of the relation (30) into equation (6) yields

$$\frac{\partial T(x,\psi)}{\partial x} = \frac{k}{\rho g c_p}\sqrt{\frac{2\tau_w(x)}{\mu}}\frac{\partial}{\partial\psi}\left[\sqrt{\psi}\frac{\partial T(x,\psi)}{\partial\psi}\right]. \tag{31}$$

Lighthill has solved this partial differential equation by use of Heaviside's operational method in reference 12 and has obtained the relation

$$q_w(x) \equiv -k\frac{\partial T(x,0)}{\partial y} = k\left(\frac{Pr\rho}{9\mu^2}\right)^{1/3}\frac{\sqrt{\tau_w(x)}}{\left(\frac{1}{3}\right)!}\left[\frac{T_w(0)-T_o}{\left(\int_o^x \tau_w^{1/2}(\xi)d\xi\right)^{1/3}} + \right.$$

$$\left. + \int_{\xi=0}^{\xi=x}\frac{dT_w(\xi)}{d\xi}\frac{d\xi}{\left(\int_{z=\xi}^{z=x}\tau_w^{1/2}(z)dz\right)^{1/3}}\right]. \tag{32}$$

For a vicinity of the stagnation point, an exact solution of the Navier-Stokes differential equations yields

$$\tau_w(x) = 1.2326\left(c\frac{u_\infty}{L}\right)^{3/2}\sqrt{\mu\rho}\,x, \tag{33}$$

according to p. 70-73 of reference 19. If the relations (13) through (15) and the usual definition

$$c_f(x) = \frac{\tau_w(x)}{\rho u_\infty^2/2} \tag{34}$$

of the wall friction coefficient are employed, the following equations may be derived:

$$Nu_1(0) = 0.660\,Pr^{1/3}Re_1^{1/2}\sqrt{c} \quad \text{and} \tag{35}$$

$$\frac{Nu_1(x)}{Nu_1(0)} = \frac{0.647}{\sqrt{c}}\left[\frac{\sqrt{c_f(x)Re_1^{1/2}}}{\left(\int_0^x \sqrt{c_f(\xi)Re_1^{1/2}}\, d\frac{\xi}{L}\right)^{1/3}} + \right.$$

$$\left. + \sqrt{c_f(x)Re_1^{1/2}} \int_{\xi=0}^{\xi=x} \frac{d}{d\frac{\xi}{L}}\left(\frac{T_w(\xi)-T_o}{T_w(0)-T_o}\right) \frac{d\frac{\xi}{L}}{\left(\int_{z=\xi}^{z=x} \sqrt{c_f(z)Re_1^{1/2}}\, d\frac{z}{L}\right)^{1/3}}\right]. \quad (36)$$

V. APPLICATION OF THE HIGH PRANDTL NUMBER METHOD TO CASES FOR WHICH SIMILARITY SOLUTIONS EXIST

The wall shear stress becomes in case of the velocity distribution (19)

$$\tau_w(x) = \left(\frac{u_\infty C}{L^m}\right)^{3/2} (\rho\mu)^{1/2} f_w''(m)\, x^{\frac{3m-1}{2}} \quad (37)$$

Numerical results for the function $f_w''(m)$ have been derived in references 5,9, and 12 and are represented in figure 2 by disregarding a few inconsistent numbers from reference 9. Equation (32) yields for constant wall temperature

$$q_w(x) = 0.538\, \frac{k}{x}\, [T_w(0)-T_o]Pr^{1/3}Re_2^{1/2}(x)\left[\frac{3}{4}\,(m+1)\, f_w''(m)\right]^{1/3} \quad (38)$$

and the heat transfer parameter, which is defined in the relations (20), takes the form

$$\frac{Nu_2(x)}{\sqrt{Re_2(x)}} = 0.538\, Pr^{1/3}\left[\frac{3}{4}\,(m+1)\, f_w''(m)\right]^{1/3} \quad (39)$$

Equation (32) becomes in case of the power laws (19) for $u_e(x)$ and $T_w(x)-T_o$, i.e., in case of variable wall temperature,

$$q_w(x) = 0.538 \frac{k}{x}[T_w(x)-T_o]\ Pr^{1/3} Re_2^{1/2}(x) \left[\frac{3}{4}(m+1)\ f''_w(m)\right]^{1/3} nx^{-n+\frac{m+1}{4}} J_2(x), \tag{40}$$

where

$$J_2(x) = x^{n-\frac{m+1}{4}} \int_{\frac{\xi}{x}=0}^{\frac{\xi}{x}=1} \left(\frac{\xi}{x}\right)^{n-1} \left[1-\left(\frac{\xi}{x}\right)^{\frac{3}{4}(m+1)}\right]^{-1/3} d\,\frac{\xi}{x}\,. \tag{41}$$

The heat transfer parameter, which is defined in the equations (20), then takes the form

$$\frac{Nu_2(x)}{\sqrt{Re_2(x)}} = 0.538 \left[\frac{3}{4}(m+1)\ f''_w(m)\right]^{1/3} Pr^{1/3} nx^{-n+\frac{m+1}{4}} J_2(x) = Pr^{1/3} B_2(m,n), \tag{42}$$

where $B_2(m,n)$ is independent of x as is seen by comparison of equations (41) and (42). The function J_2 can be evaluated analytically in closed form for special pairs of values of m and n. For example, $B_2(3,3) = 1.316$ by use of the function $f''_w(m)$ in Fig. 2.

Both the low and the high Prandtl number methods and the exact solution for any Prandtl number yield expressions for $Nu_2(x)/\sqrt{Re_2(x)}$ which are independent of x as the comparison of equations (21), (25), (29), (39), and (42) shows. The functions $Nu_2(x)/\sqrt{Re_2(x)}$ are represented in Fig. 3 versus m for n = 0 and Pr = 0.7. The three methods, therefore, yield identical results for $Nu_2(x)/Nu_2(x^*)$, where x^* is any reference value.

VI. THE FUNCTIONS $u_e(x)$ AND $c_f(x)$ FOR THE INVESTIGATED CASES

Incompressible potential theory yields the velocity distribution

$$u_e(\varphi) = 2u_\infty \sin\varphi \tag{43}$$

at the surface of the circular cylinder presented in Fig. 5. In the vicinity of the stagnation point of this cylinder, $u_e(x_o) = 4u_\infty x_o/L$, where the coordinate x_o measures along the circumference of the circular cross section, which possesses the diameter L = 2R; c then has the value c = 4. According to references 8, the velocity distribution

$$\frac{u_e(x)}{u_\infty} = 3.6314\,\frac{x}{L} - 2.1709\left(\frac{x}{L}\right)^3 - 1.5144\left(\frac{x}{L}\right)^5 + \ldots \quad \text{with } c = 3.6314 \tag{44}$$

follows from the measured pressure distribution around a circular cylinder in an airstream with the Reynolds number 19,000.

The functions

$$\xi_1 = a_1 \cos\varphi \text{ and } \eta_1 = b_1 \sin\varphi \tag{45}$$

$$\text{with } a_1 = R\left(1+\frac{a^2}{R^2}\right),\ b_1 = R\left(1-\frac{a^2}{R^2}\right),\ \text{and } 0 \le a \le R$$

represent the conformal mapping of the $\xi_1 - \eta_1$ plane, Fig. 6, on the $\xi_0 - \eta_0$ plane, Fig. 5. The corresponding relation between the complex stream functions in the $\xi_1 - \eta_1$ plane and in the $\xi_0 - \eta_0$ plane yields (e.g., p. 121 of reference 18)

$$\frac{u_e(\varphi(x))}{u_\infty} = \frac{1+\lambda}{\sqrt{1+\lambda^2 \operatorname{ctg}^2\varphi}}, \tag{46}$$

where $\lambda = \dfrac{b_1}{a_1}$. In a vicinity of the stagnation point $x = \varphi = 0$,

$$\frac{u_e(\varphi)}{u_\infty} = \frac{1+\lambda}{\lambda}\varphi = \frac{1+\lambda}{\lambda}\frac{x_o}{R} \text{ and } \frac{x_o}{R} = \frac{1+\lambda}{2\lambda}\frac{x_1}{R} = \frac{1+\lambda}{2\lambda}\frac{x_1}{a_1}\left(1+\frac{1-\lambda}{1+\lambda}\right) = \frac{1}{\lambda}\frac{x_1}{a_1}, \tag{47}$$

because of $a^2/R^2 = (1-\lambda)/(1+\lambda)$. Equation (47) yields

$$\frac{u_e(x_1)}{u_\infty} = 2\,\frac{1+\lambda}{\lambda^2}\frac{x_1}{L} \qquad \text{for } x_1 \ll 1, \tag{48}$$

where $L = 2a_1$. The functions (43) and (44) for the circular cross section and the function (46) for several elliptic cross sections are presented in Fig. 7.

Fig. 8, which represents data taken from reference 4, shows the surface velocity distribution $u_e(x)/u_\infty$ in planar incompressible flow for a single airfoil, $t/L = \infty$, and for the same airfoil in a cascade with $t/L = 0.5$.

According to p. 136 of ref. 19, the expression

$$c_f(x)\sqrt{Re_1} \equiv \frac{\tau_w(x)}{\frac{\rho}{2}u_\infty^2}\sqrt{Re_1} = 9.861\,\frac{x}{\frac{L}{2}} - 3.863\left(\frac{x}{\frac{L}{2}}\right)^3 + 0.413\left(\frac{x}{\frac{L}{2}}\right)^5 - \ldots \tag{49}$$

for the wall friction coefficient follows from a series expansion of the solution for the laminar incompressible boundary layer in case of a circular cylinder with the velocity distribution (43). Fig. 9 presents $c_f(x)\sqrt{Re_1}$ versus x/L as following from the equation (37) for a flat plate with m = 0, from equation (49) for the circular cylinder, and from a Kármán-Pohlhausen analysis for the ellipses with the ratios 1:2 and 1:4 of the minor and major axes (see p. 217 of ref. 19).

VII. DISCUSSION OF THE RESULTS

The heat flux equation

$$q_w(x) = -k\,\frac{\partial T(x,0)}{\partial y} = \rho g c_p\,\frac{d}{dx}\int_0^\infty u(x,y)[T(x,y) - T_o]\,dy \tag{50}$$

of the temperature boundary layer is obtained by integration of the energy equation (3) across the boundary layer from y = 0 to the outer edge. Since the temperature as a function of y cannot possess a point of inflection in problems of convective heat transfer with negligible frictional heating in the absence of mass transfer at the wall, equation (50) shows that the wall heat transfer rate $q_w(x)$ increases together with the level of the velocity component u(x,y) in the vicinity of the wall.

If a heat transfer problem of the type being considered with $0 < Pr < \infty$ is treated by use of the low Prandtl number method, u(x,y) is replaced by $u_e(x)$, where $u(x,y) \leq u_e(x)$. The error of the low Prandtl number method, therefore, is positive and in general increases together with the boundary layer thickness, i.e., with x. The error then should take a minimum value at the forward stagnation point x = 0.

If a heat transfer problem with $0 < Pr < \infty$ is treated by use of the high Prandtl number method, u(x,y) is replaced by its wall tangent $y\tau_w(x)/\mu$. The error of the high Prandtl number method, therefore, is positive between the forward stagnation point x = 0 and a point close to the point $x = x_m$ of minimum pressure; since u(x,y) as a function of y has a point of inflection for $x \geq x_m$, the error is negative in the range $x_m < x < x_s$, where x_s is the point of separation or transition of the laminar boundary layer.

The x-independent relationship (15) between Nu_1 and $q_w(x)$ in case of constant wall temperature T_w shows that these conclusions on the deviations of the low and the high Prandtl number methods from exact solutions are valid for $Nu_1(x)$ as well as for $q_w(x)$. Therefore, the low Prandtl number overestimates both $Nu_1(x)/\sqrt{Re_1}$ and $Nu_1(x)/Nu_1(0)$ at rates which increase together with x. The high Prandtl number method overestimates $Nu_1(x)/\sqrt{Re_1}$ in the range $0 \leq x < x_m$ and underestimates $Nu_1(x)/\sqrt{Re_1}$ for $x > x_m$. The comparison of the two methods under discussion to exact similarity solutions in Fig. 3 confirms these conclusions. In particular, the error of the high Prandtl number method has different signs for $m > 0$ and for $m < 0$.

If the inevitable small inaccuracies of the quoted and of the calculated results are taken into account, figures 10 through 15 confirm for constant wall temperature that the low Prandtl number method overestimates $Nu_1(x)/Nu_1(0)$ at a rate which increases together with x. The presented examples show that the high Prandtl number method underestimates $Nu_1(x)/Nu_1(0)$ for $0 \leq x < x_m$ in case of slender bodies. These conclusions still are valid between $x = 0$ and a point close to $x = \xi$ where ξ is defined by $T_w(\xi) = T_o$ in case of variable wall temperature $T_w = T_w(x)$ (Figures 16 - 18).

The presented results, in particular the comparison of Figures 10 and 19 or 13 and 20, show for both the low and the high Prandtl number methods that the deviation of $Nu/\sqrt{Re}$ from pertinent exact or approximate solutions can be represented as the product of large x-independent contributions, inherent to the methods, and of small x-dependent modifications, where only the latter part remains in $Nu(x)/Nu(0)$. This explains why it is advantageous to employ the result $Nu(x)/Nu(0)$ of the low or the high Prandtl number methods rather than their result $Nu(x)/\sqrt{Re}$.

If $T_w(x) = \text{const.}$ in a small vicinity of the forward stagnation point $x = 0$, the evaluation of exact similarity solutions, e.g., equation (21), furnishes exact expressions for $Nu_1(0)/\sqrt{Re_1}$, which depend correctly on Pr. The exact factor $Nu_1(0)/\sqrt{Re_1}$ times the result $Nu_1(x)/Nu_1(0)$ of the low or the high Prandtl number methods yields satisfactory approximations to the exact solution for $Nu_1(x)/\sqrt{Re_1}$, and this in the total range of Prandtl numbers.

Contrary to other calculation methods for the wall heat transfer as a function of x in case of arbitrary cross sections, both the low and the high Prandtl number method result in closed-form solutions. A comparison of equations (18) and (36) shows that the numerical evaluation of the high Prandtl number method is more involved than the one of the low Prandtl number method, in particular, if $T_w(x) \neq \text{const.}$ Also, the input function $u_e(x)$ of the low Prandtl number method follows from ideal fluid flow theory, whereas the high Prandtl number method depends on the wall friction coefficient $c_f(x)$, which is a result of boundary layer analysis.

VIII. CONCLUSIONS

Both the low and the high Prandtl number methods yield closed form solutions for the wall heat transfer in the two limiting cases $Pr \to 0$, achieved through $\mu \to 0$, and $Pr \to \infty$, respectively. The error is investigated which is due to approximating a given heat transfer problem with $0 < Pr < \infty$ by the limiting problems. The results for $Nu_1(x)/Nu_1(0)$ of the low or the high Prandtl number methods yield significantly closer approximations than their results for $Nu_1(x)/\sqrt{Re_1}$. The expressions $Nu_2(x)/Nu_2(x^*)$ as obtained from the low and the high Prandtl number methods and from exact boundary layer solutions coincide in the similarity case defined by the power laws (19) for $u_e(x)$ and $T_w(x) - T_o$. It is shown theoretically and confirmed by the numerical results that the low Prandtl number method yields an upper limit for both $Nu_1(x)/\sqrt{Re_1}$ and $Nu_1(x)/Nu_1(0)$. Theoretical conclusions and the presented data yield the result that the high Prandtl number method overestimates $Nu_1(x)/\sqrt{Re_1}$ in the region of accelerated flow and underestimates $Nu_1(x)/\sqrt{Re_1}$ in the region of decelerated flow. The presented examples show for slender bodies that the high Prandtl number method furnishes a lower limit for $Nu_1(x)/Nu_1(0)$ in the region of accelerated flow. Since exact solutions for $Nu_1(0)/\sqrt{Re_1}$ exist at the stagnation point $x = 0$ for a wide range of Prandtl numbers, if the temperature $T_w = \text{const.}$ in a small vicinity of the stagnation point, the product of the exact factor $Nu_1(0)/\sqrt{Re_1}$ and of the results $Nu_1(x)/Nu_1(0)$ of the low or the high Prandtl number methods, respectively, yields satisfactory approximations for $Nu_1(x)/\sqrt{Re_1}$ in the range $0 \leq Pr \leq \infty$. The amount of work involved in calculating the input function $u_e(x)$ and in evaluating the low Prandtl number method is significantly smaller than the amount of work involved in solving the boundary layer equations for the input function $c_f(x)\sqrt{Re_1}$ and in evaluating the high Prandtl number method.

APPENDIX

THE SOLUTION OF THE EQUATIONS (7) - (10)

The differential equation (7) together with the initial and boundary conditions (8) - (10) may be solved by the expression

$$T(\emptyset,\psi) - T_o = \int_{\eta=0}^{\eta=\emptyset} [T_w(\eta)-T_o] \frac{\partial}{\partial \emptyset} F(\emptyset-\eta,\psi)\, d\eta, \tag{A-1}$$

according to p. 62 of reference 1, where η is a dummy variable for $\emptyset$ in the limits $0 \leq \eta \leq \emptyset$. The function

$$F(\emptyset-\eta,\psi) = \frac{2}{\sqrt{\pi}} \int_{\frac{\psi}{2\sqrt{A(\emptyset-\eta)}}}^{\infty} e^{-\eta^2}\, d\eta \qquad \text{with } A = \frac{k}{\rho g c_p} \tag{A-2}$$

is related to the error integral $\operatorname{erf} x = \frac{2}{\sqrt{\pi}} \int_o^x e^{-\zeta^2}\, d\zeta$. Both $F(\emptyset-\eta,\psi)$ and its derivatives are well defined for $\eta < \emptyset$ and their limits exist as $\eta \to \emptyset$ for $\psi > 0$; at the point $\psi = 0$ and $\eta = \emptyset$, however, these functions do not possess unique limits. The equations (A-1) and A-2 yield the relation

$$T(\emptyset,\psi)-T_o = \frac{\psi}{2\sqrt{A\pi}} \int_{\eta=0}^{\eta=\emptyset} [T_w(\eta)-T_o] \frac{\exp[-\psi^2/4A(\emptyset-\eta)]}{(\emptyset-\eta)^{3/2}}\, d\eta \qquad \text{for } \psi > 0\,. \tag{A-3}$$

It is immediately seen that the relation (A-3) satisfies the conditions (8) and (10). Since the derivatives of (A-3) exist for $\psi > 0$, it can be shown for $\psi > 0$ that the relation (A-3) satisfies the differential equation (7). It is shown in the following paragraph that the relation (A-3) satisfies the remaining boundary condition (9)if $T_w(0) = T_o$.

Equation (A-3) becomes

$$T(\emptyset,\psi)-T_o = \frac{2}{\sqrt{\pi}} \int_{\mu=\frac{\psi}{2\sqrt{A\emptyset}}}^{\infty} [T_w(\emptyset-\psi^2/4A\mu^2)-T_o]\, e^{-\mu^2}\, d\mu \tag{A-4}$$

when the coordinate transformation

$$\mu = \frac{\psi}{2\sqrt{A(\phi-\eta)}} \tag{A-5}$$

is introduced, which relates the independent variables η and μ and which exists if $\phi > 0$ and $\psi > 0$. The integrand in equation (A-4) possesses the following finite discontinuity at the point defined by $\mu = 0$ and $\psi = 0$:

$$\lim_{\psi \to 0} T_w\left(\phi - \frac{\psi^2}{4A\mu^2}\right) - T_o = \begin{cases} T_w(\phi)-T_o & \text{for } \mu > \dfrac{\psi}{2\sqrt{A\phi}} \text{ and } \phi > 0 \\ \left|T_w(0)-T_o\right| = 0 < \left|T_w(\phi)-T_o\right| & \text{for } \mu = \dfrac{\psi}{2\sqrt{A\phi}} \text{ and } \phi > 0; \end{cases} \tag{A-6}$$

The integral in equation (A-4) can be expressed as the sum of the "main part" pertaining to the range $\epsilon + \frac{\psi}{2\sqrt{A\phi}} \leq \mu \leq \infty$, where $0 < \epsilon \ll 1$, and of the "remainder" for the range $\frac{\psi}{2\sqrt{A\phi}} \leq \mu \leq \epsilon + \frac{\psi}{2\sqrt{A\phi}}$. If the integrand in the remainder is replaced by its upper bound $T_w(\phi)-T_o$, according to the relations (A-6), it is seen for $\phi > 0$ that the resulting upper bound of the remainder tends to zero together with ϵ at any value of ψ. Because of

$$\int_0^\infty e^{-\mu^2}\, d\mu = \sqrt{\pi}/2,$$

the main part then tends to the limit $T_w(\phi)-T_o$ when ϵ and ψ tend to zero independently of one another; i.e., the boundary condition (9) is satisfied by the relation (A-3).

The integration by parts is valid in the right-hand side of equation (A-3) since the integrals converge uniformly for $\psi > 0$ and $0 \leq \phi < \infty$. Because of $\partial F/\partial\phi = -\partial F/\partial\eta$ and $\lim_{\eta \to \phi} F(\phi-\eta,\psi) = 0$, equation (A-3) then becomes

$$T(\phi,\psi)-T_o = \int_{\eta=0}^{\eta=\phi} \frac{dT_w(\eta)}{d\eta} F(\phi-\eta,\psi)\, d\eta \qquad \text{for } \psi > 0 \text{ and } T_w(0) = T_o. \tag{A-7}$$

Since equation (A-7) may be differentiated if $\psi > 0$,

$$\frac{\partial T(\phi,\psi)}{\partial \psi} = -\frac{2}{\sqrt{\pi}} \int_{\eta=0}^{\eta=\phi} \frac{dT_w(\eta)}{d\eta} \frac{\exp[-\psi^2/4A(\phi-\eta)]}{2\sqrt{A(\phi-\eta)}} d\eta \quad \text{for } \psi > 0 \text{ and } T_w(0) = T_o. \tag{A-8}$$

The integrand in equation (A-8) possesses a finite discontinuity at the point defined by $\eta = \phi$ and $\psi = 0$. Because of $0 \leq \exp[-\psi^2/4A(\phi-\eta)] < 1$, it may be shown by an argument following the one presented above that the limiting form of the equation as $\psi \to 0$ is

$$\frac{\partial T(\phi,0)}{\partial \psi} = -\sqrt{\frac{\rho g c_p}{\pi k}} \int_{\eta=0}^{\eta=\phi} \frac{dT_w(\eta)}{d\eta} \frac{d\eta}{\sqrt{\phi-\eta}} \quad \text{for } \phi \geq 0. \tag{A-9}$$

For constant wall temperature, $T_w(\phi) - T_o \equiv T_w(0) - T_o = \text{const.}$, equation (A-1) becomes, because of $\partial F/\partial\phi = -\partial F/\partial\eta$,

$$T(\phi,\psi)-T_o = -[T_w(0)-T_o]\, F(\phi-\eta,\psi)\Big|_{\eta=0}^{\eta=\phi} = \frac{2}{\sqrt{\pi}}[T_w(0)-T_o] \int_{\psi/2\sqrt{A\phi}}^{\infty} e^{-\zeta^2} d\zeta \tag{A-10}$$

except at the point defined by $\phi = 0$ and $\psi = 0$. Equation (A-10) satisfies the initial and boundary conditions (8) - (10) because of $\int_0^{\infty} e^{-\zeta^2} d\zeta = \frac{\sqrt{\pi}}{2}$.

Also,

$$\frac{\partial T(\phi,\psi)}{\partial \psi} = \frac{-2}{\sqrt{\pi}}[T_w(0)-T_o] \frac{\exp[-\psi^2/4A\phi]}{2\sqrt{A\phi}} \quad \text{and} \tag{A-11}$$

$$\frac{\partial T(\phi,0)}{\partial \psi} = -\sqrt{\frac{\rho g\, c_p}{\pi k}} \frac{T_w(0)-T_o}{\sqrt{\phi}} \quad \text{for } \phi > 0. \tag{A-12}$$

If $T_w(0) \neq T_o$, the temperature gradient $\partial T/\partial\psi$ does not exist at $\phi = \psi = 0$. This singularity of the solution is due to the incompatibility of the initial condition (8) and the boundary condition (9) in case of $T_w(0) \neq T_o$; because of the first part of equation (17), the limit

$\lim_{\phi \to 0} u_e(\phi) \frac{\partial T(\phi,\psi)}{\partial \psi}$ is finite. The equations (A-9) and (A-12), therefore, yield the following expression for the temperature gradient $\partial T/\partial y$ at the wall y = 0:

$$\frac{\partial T(x,0)}{\partial y} = \frac{\partial T(x,0)}{\partial \psi} \frac{\partial \psi}{\partial y} = - \sqrt{\frac{\rho g c_p}{\pi k}} u_e(x) \left[\frac{T_w(0) - T_o}{\sqrt{\phi(x)}} + \int_{\eta=0}^{\eta=\phi(x)} \frac{dT_w(\eta)}{d\eta} \frac{d\eta}{\sqrt{\phi - \eta}} \right]. \tag{A-13}$$

where $\left[T_w(0) - T_o \right] / \sqrt{\phi(x)}$ corresponds to the distribution $T_{w1}(\phi) - T_o = T_w(0) - T_o = \text{const.}$ and the integral corresponds to $T_{w2}(\phi) = T_w(\phi) - T_w(0)$. Clearly, the sum $T_{w1}(\phi) - T_o + T_{w2}(\phi) = T_w(\phi) - T_o$ represents the given wall temperature distribution.

Non-dimensional wall temperature gradient $\left\{(-\sqrt{xL/Re_1})(\partial T/\partial y)_w\left[1/(T_w - T_o)\right]\right\}$ versus Prandtl number Pr for flat plate at constant wall temperature T_w in uniform flow, data taken from Fig. 1 of Ref. 14.

Curve No. 1: Result of Kármán-Pohlhausen analysis, presented in Ref. 21

Curve No. 2: Low Prandtl number approach

Curve No. 3: Low Prandtl number approach plus correction term taken from Ref. 14

The points marked by ⊙ represent the exact solution in Ref. 16.

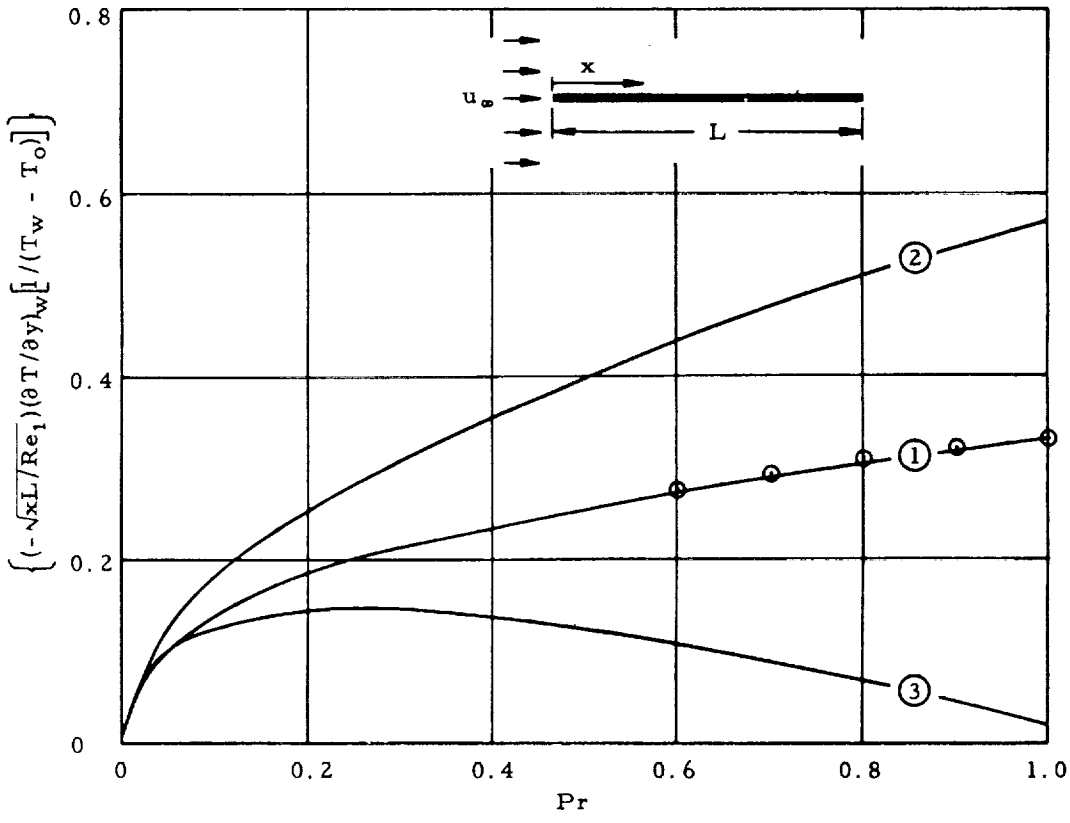

FIG. 1. NON-DIMENSIONAL WALL TEMPERATURE GRADIENT FOR FLAT PLATE

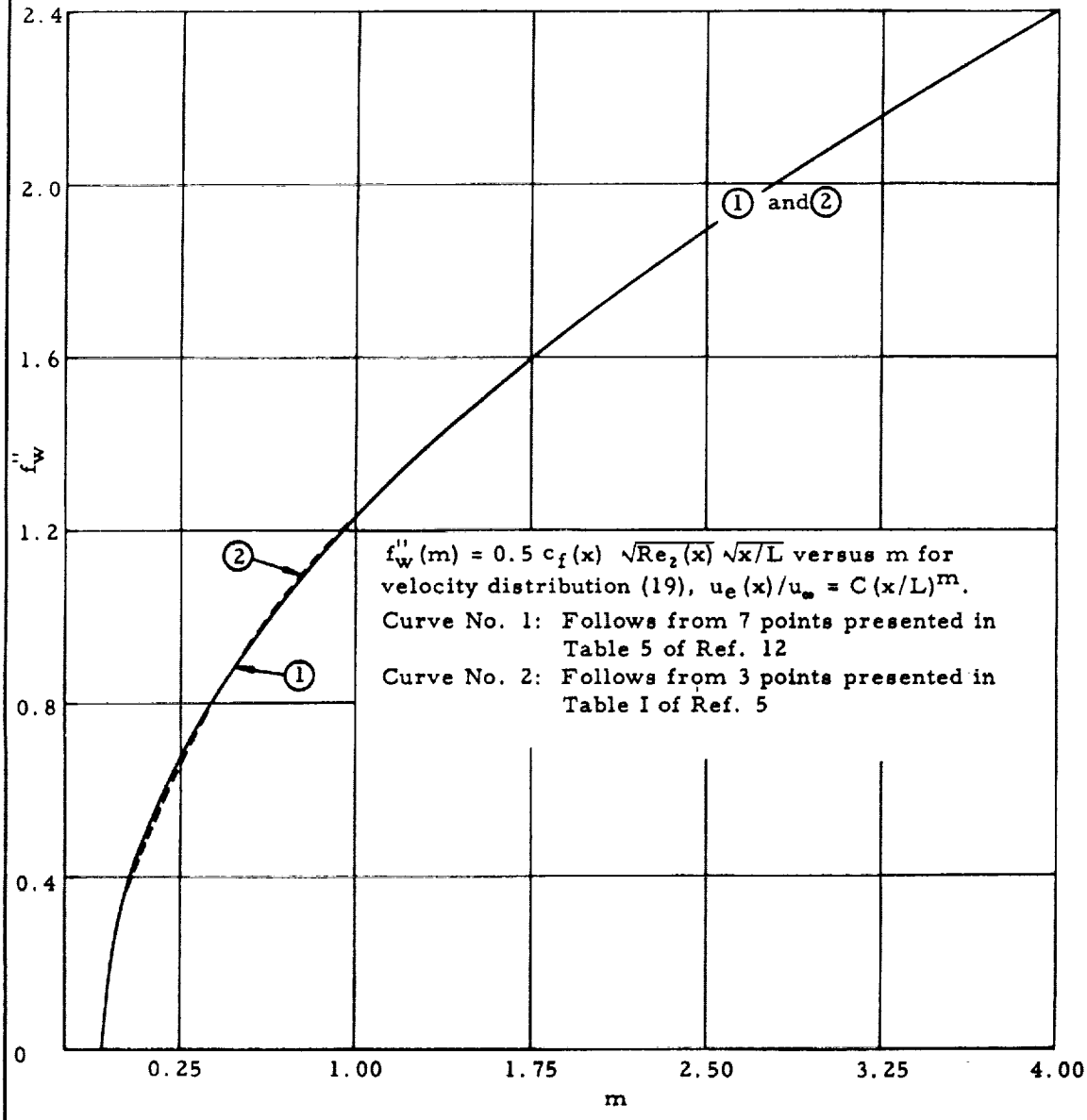

FIG. 2. NON-DIMENSIONAL FRICTION COEFFICIENT FROM EXACT SIMILARITY SOLUTIONS

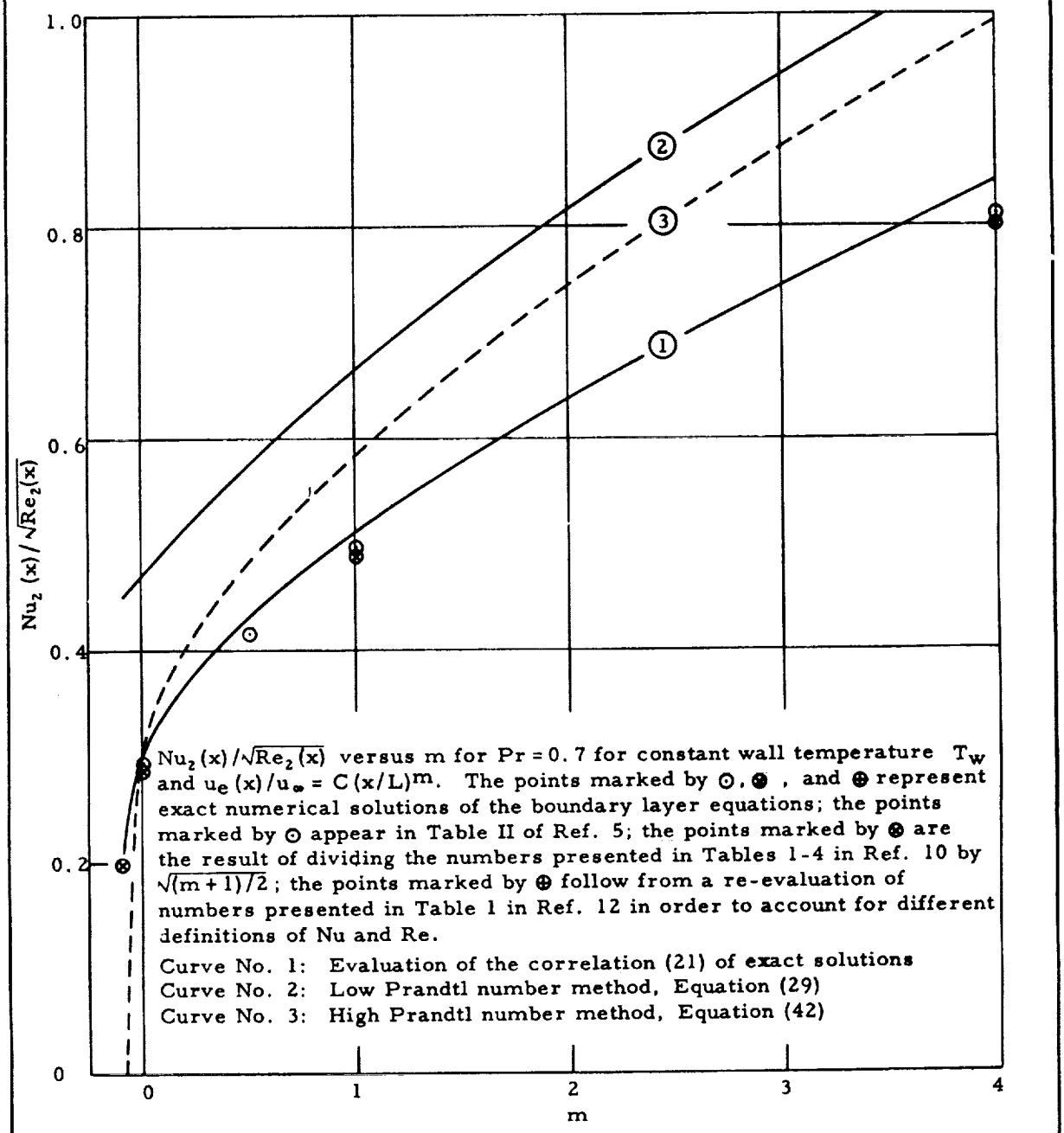

FIG. 3. $Nu_2(x)/\sqrt{Re_2(x)}$ FROM EXACT SIMILARITY SOLUTIONS

$Nu_2(x)/\sqrt{Re_2(x)Pr}$ versus Pr for a flat plate with $u_e(x) = u_\infty$ at constant wall temperature T_w.

Curve No. 1: Exact numerical solution derived in Ref. 22

Curve No. 2: Result of Kármán-Pohlhausen analysis in Ref. 21, yielding $Nu_2(x)/\sqrt{Re_2(x)Pr} = 0.529/(1 + 0.82\sqrt{Pr})$

Curve No. 3: Low Prandtl number approach, Equation (12)

Curve No. 4: Low Prandtl number approach plus correction term taken from Ref. 14, yielding $Nu_2(x)/\sqrt{Re_2(x)Pr} = 0.564 - 0.547\sqrt{Pr}$

Curve No. 5: High Prandtl number approach, Equation (32)

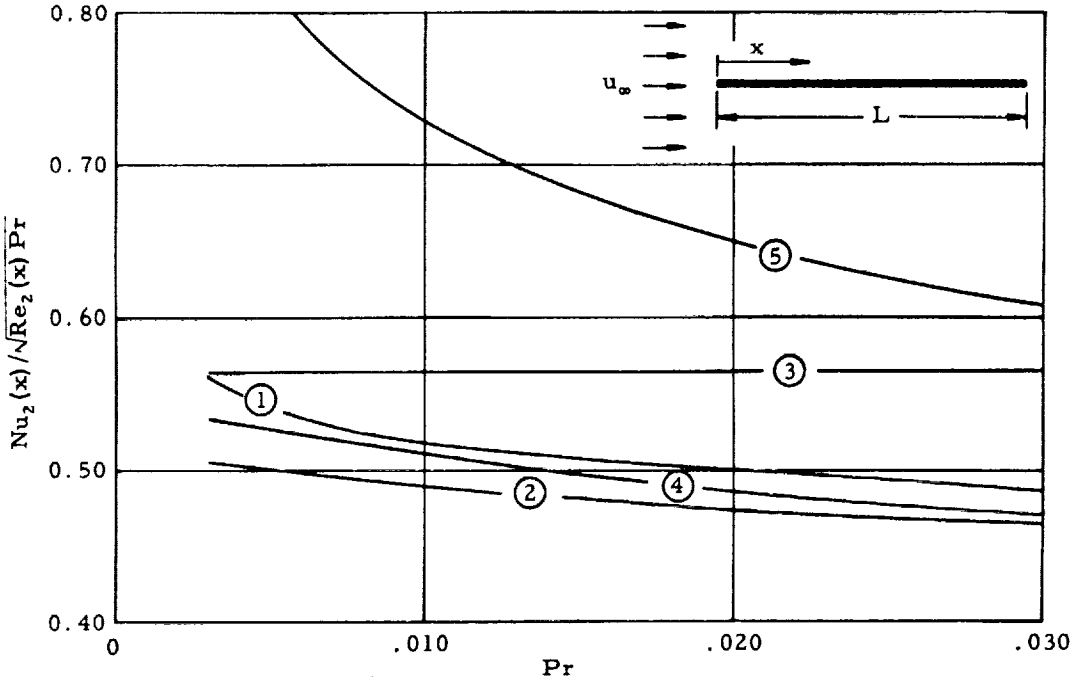

FIG. 4. $Nu_2(x)/\sqrt{Re_2(x)Pr}$ FOR FLAT PLATE

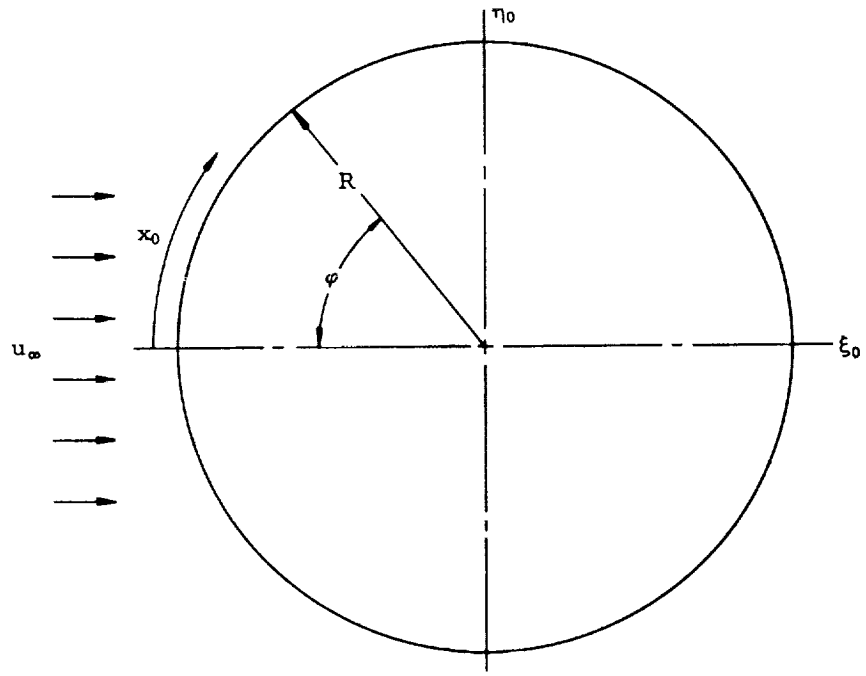

FIG. 5. CIRCULAR CYLINDER IN UNIFORM PLANAR FLOW IN THE $\xi_0 - \eta_0$ PLANE

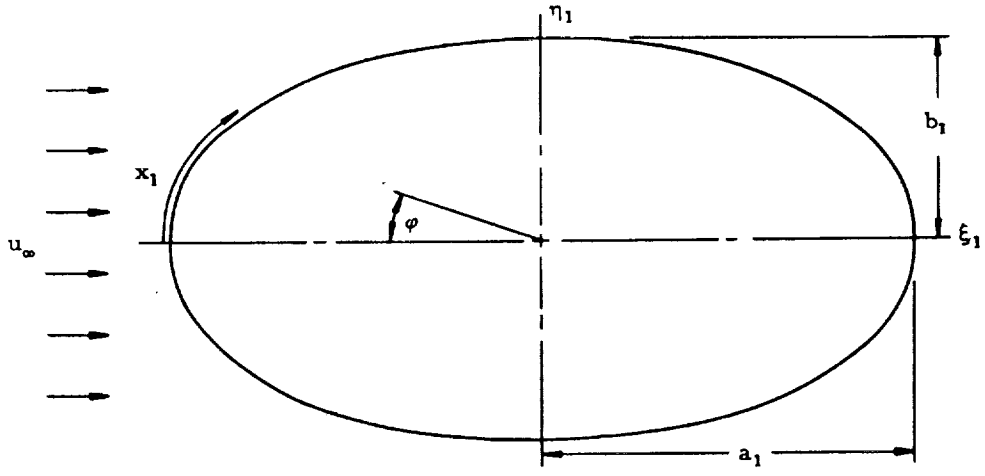

FIG. 6. ELLIPTICAL CYLINDER IN UNIFORM PLANAR FLOW IN THE $\xi_1 - \eta_1$ PLANE

$u_e(x)/u_\infty$ for several cylinders in uniform planar flow.
Curve No. 1: Evaluation of the Equation (43) for the circular cylinder, which follows from potential theory
Curve No. 2: Evaluation of the Equation (44) for the circular cylinder, which follows from measurements at Re_1 = 19,000, see Ref. 8
Curve No. 3: Evaluation of the Equation (46) for the elliptic cylinder with the ratio 1:2 of the axes
Curve No. 4: Evaluation of the Equation (46) for the elliptic cylinder with the ratio 1:4 of the axes

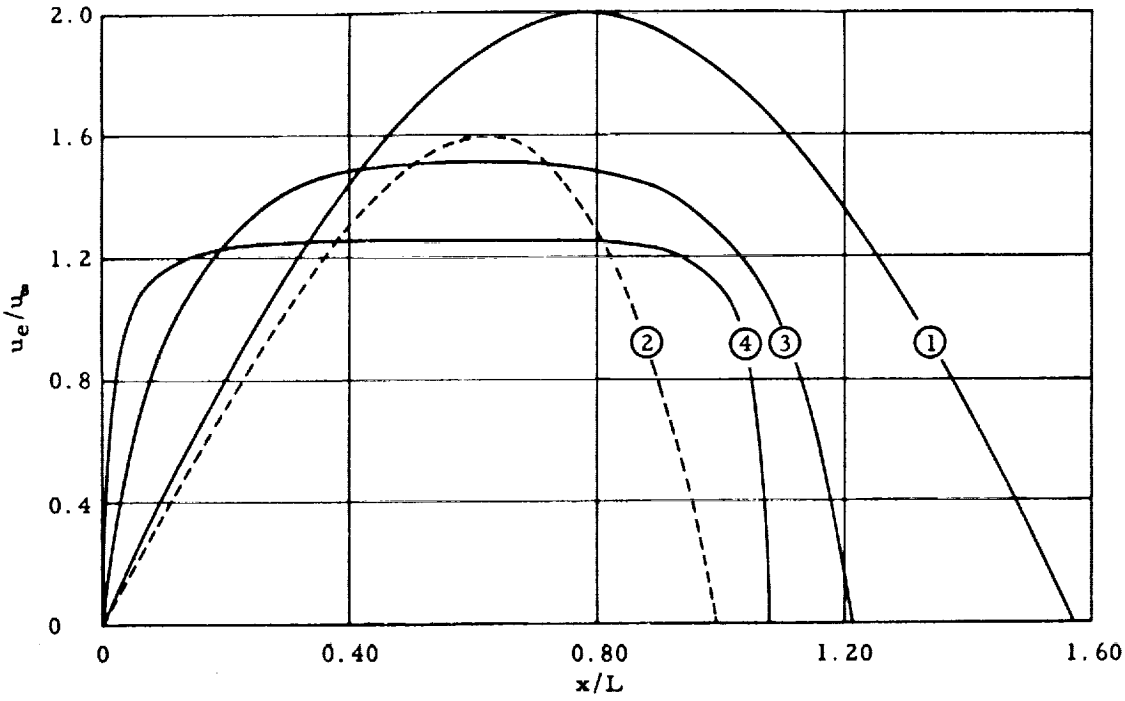

FIG. 7. VELOCITY DISTRIBUTIONS AT SURFACES OF CIRCULAR AND ELLIPTIC CYLINDERS

$u_e(x)/u_\infty$ versus x/L for airfoils in uniform planar flow, data taken from p. 98 of Ref. 4.

Curve No. 1: Single airfoil, $t/L = \infty$

Curve No. 2: Same airfoil in cascade flow with $t/L = 0.5$

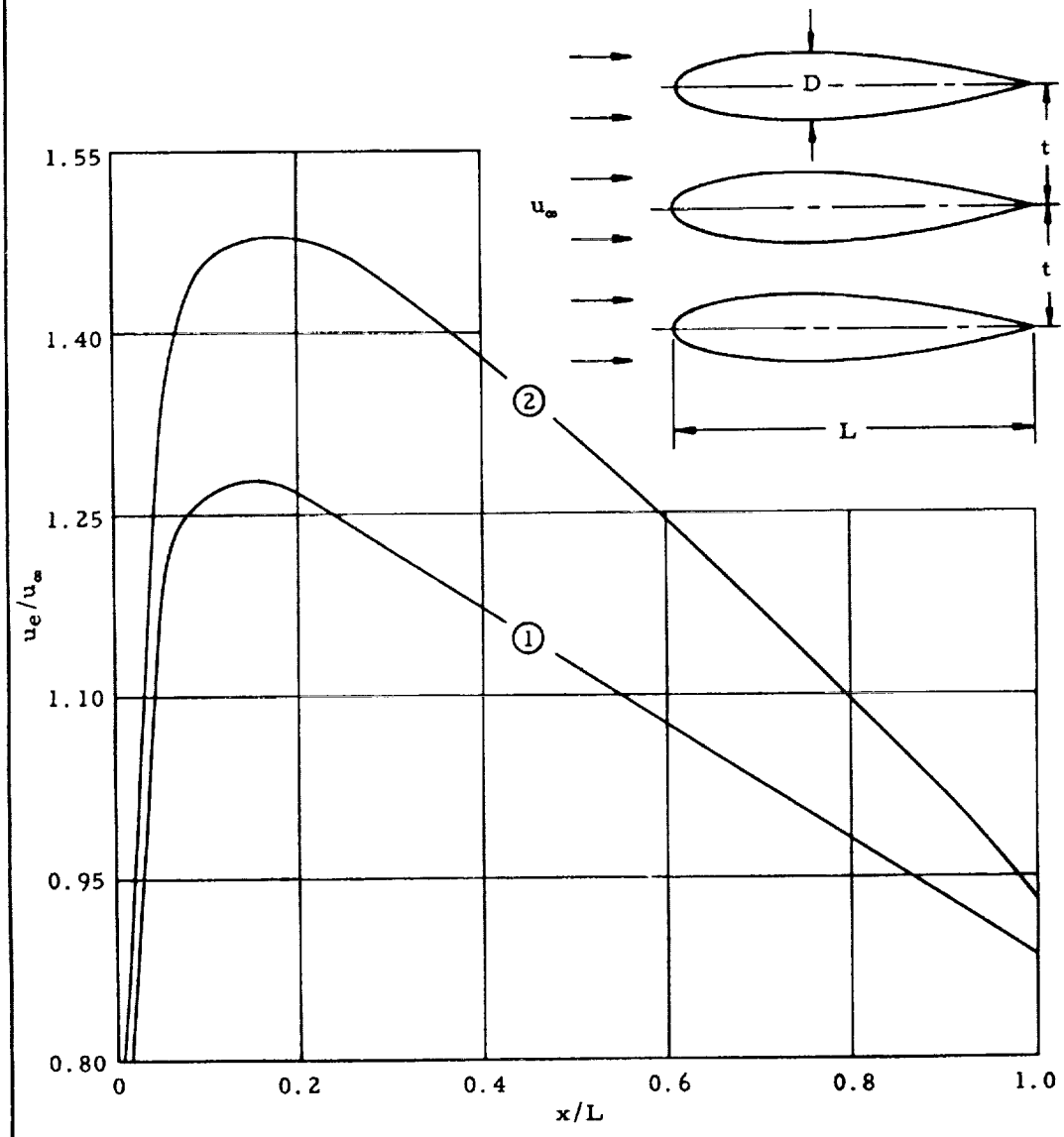

FIG. 8. VELOCITY DISTRIBUTIONS AT SURFACE OF AIRFOIL

$c_f(x)\sqrt{Re_1}$ versus x/L for laminar incompressible flow.

Curve No. 1: Evaluation of the function $c_f\sqrt{Re_1} = 2f''_w(0)\sqrt{L/x}$, which follows from Equation (37) for the flat plate, m = 0

Curve No. 2: Evaluation of Equation (49) for the circular cylinder

Curve No. 3: Result of Kármán-Pohlhausen analysis presented on p. 217 of Ref. 19 for elliptical cylinder with ratio 1:4 of axes

Curve No. 4: Result of Kármán-Pohlhausen analysis presented on p. 217 of Ref. 19 for elliptical cylinder with ratio 1:2 of axes

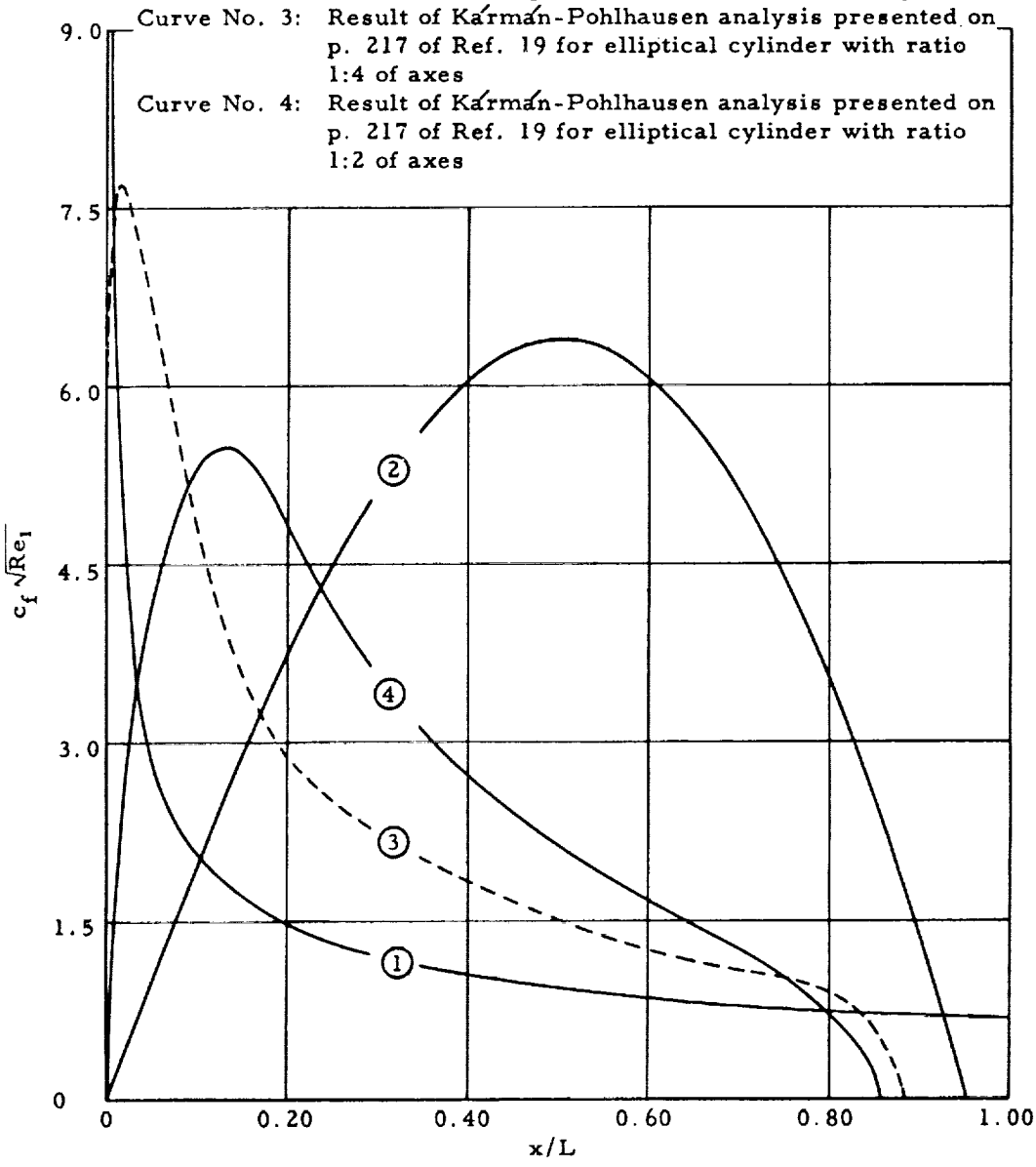

FIG. 9. FRICTION COEFFICIENT FOR FLAT PLATE, CIRCULAR, AND ELLIPTIC CYLINDER

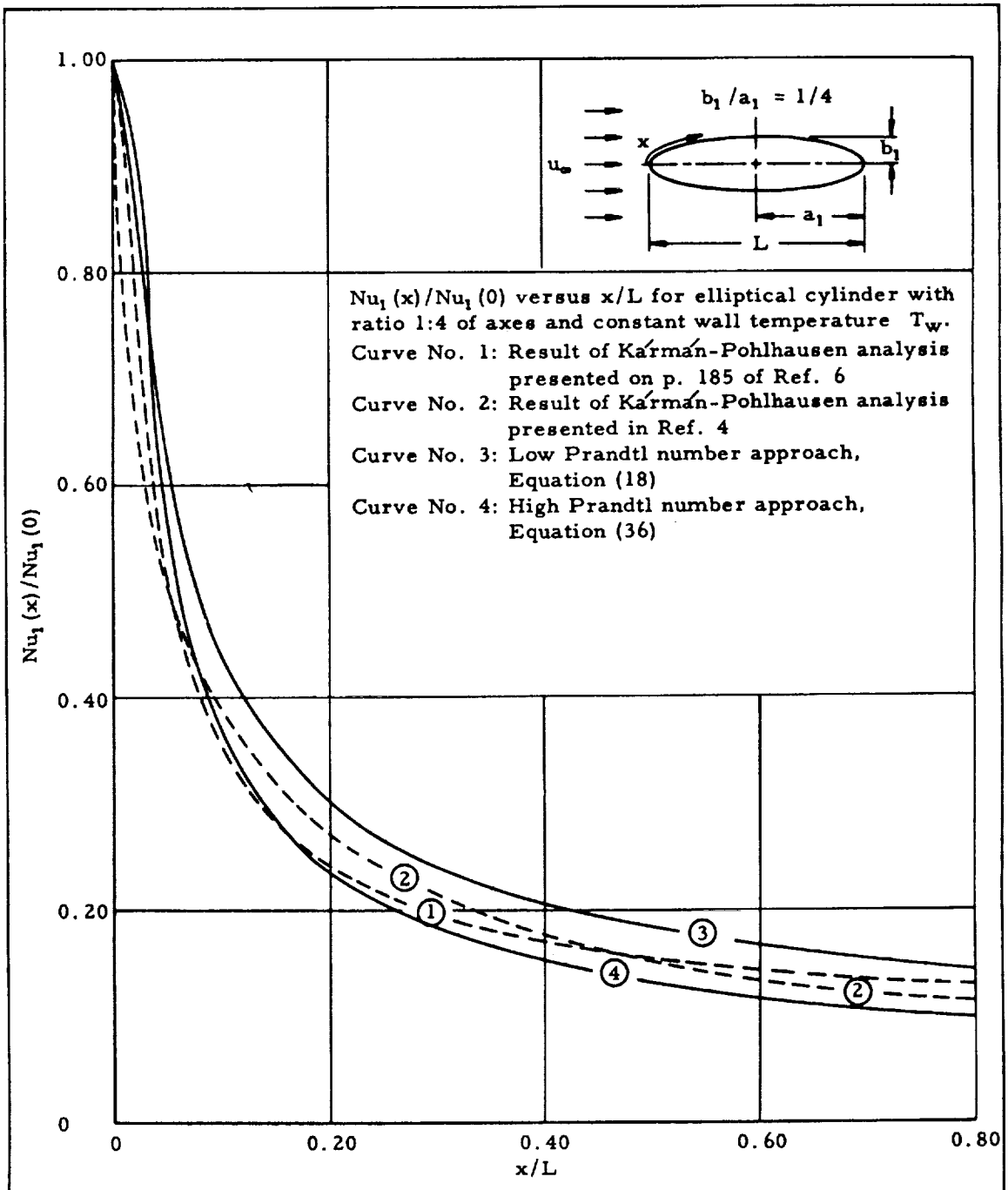

FIG. 10. $Nu_1(x)/Nu_1(0)$ FOR ELLIPTICAL CYLINDER 1:4, T_W = CONST.

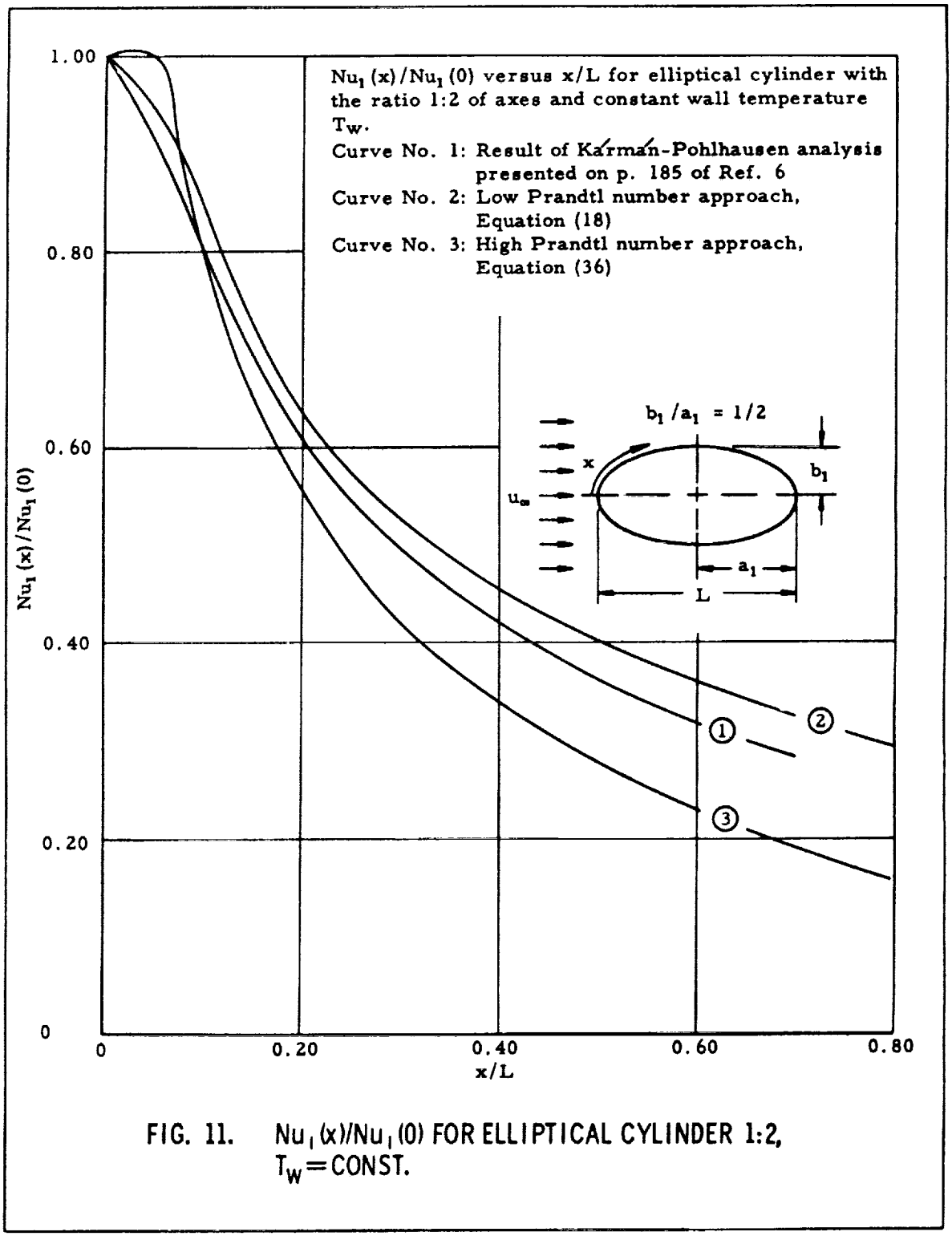

FIG. 11. $Nu_1(x)/Nu_1(0)$ FOR ELLIPTICAL CYLINDER 1:2, T_W = CONST.

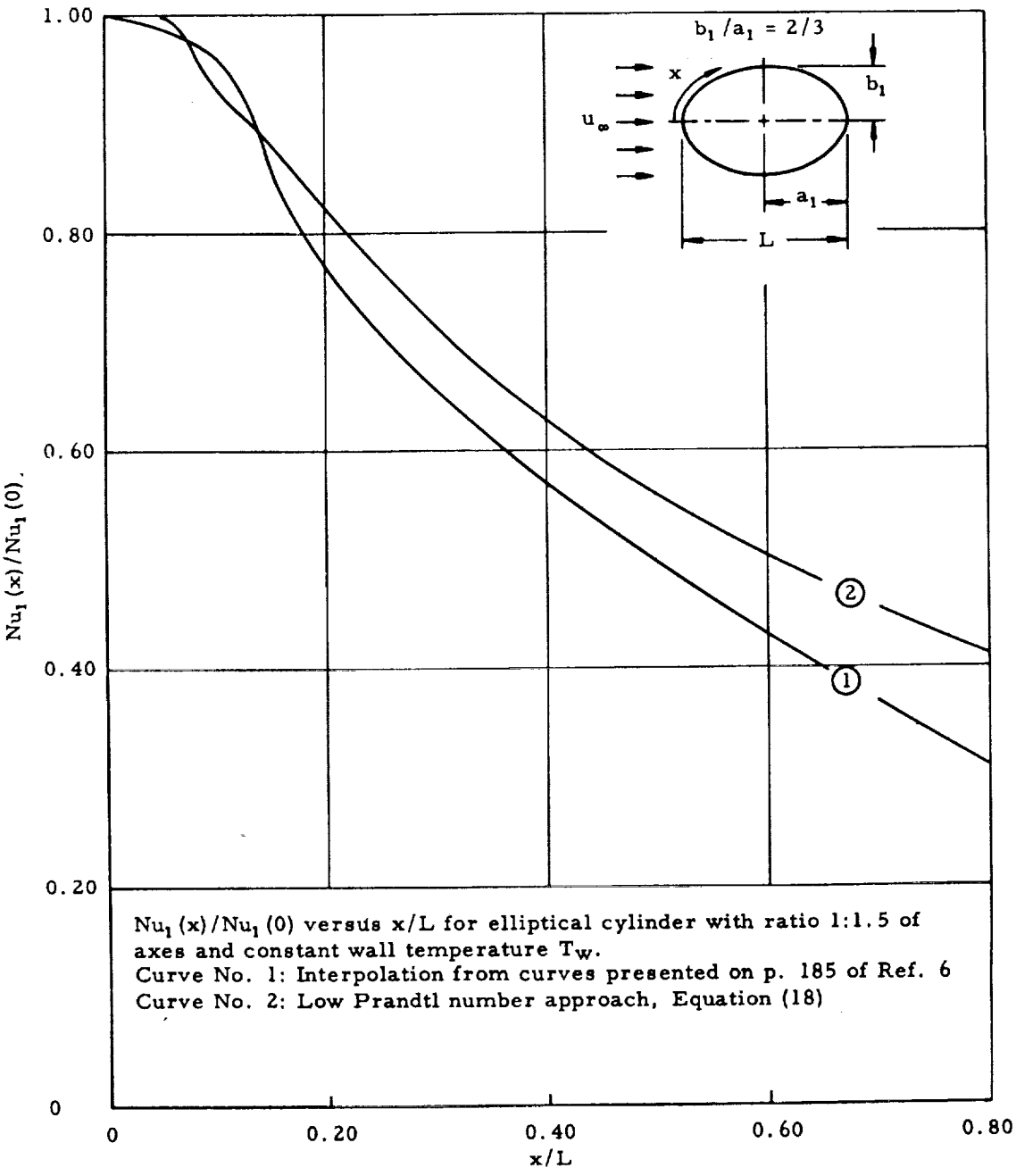

FIG. 12. $Nu_1(x)/Nu_1(0)$ FOR ELLIPTICAL CYLINDER 1:1.5, T_W = CONST.

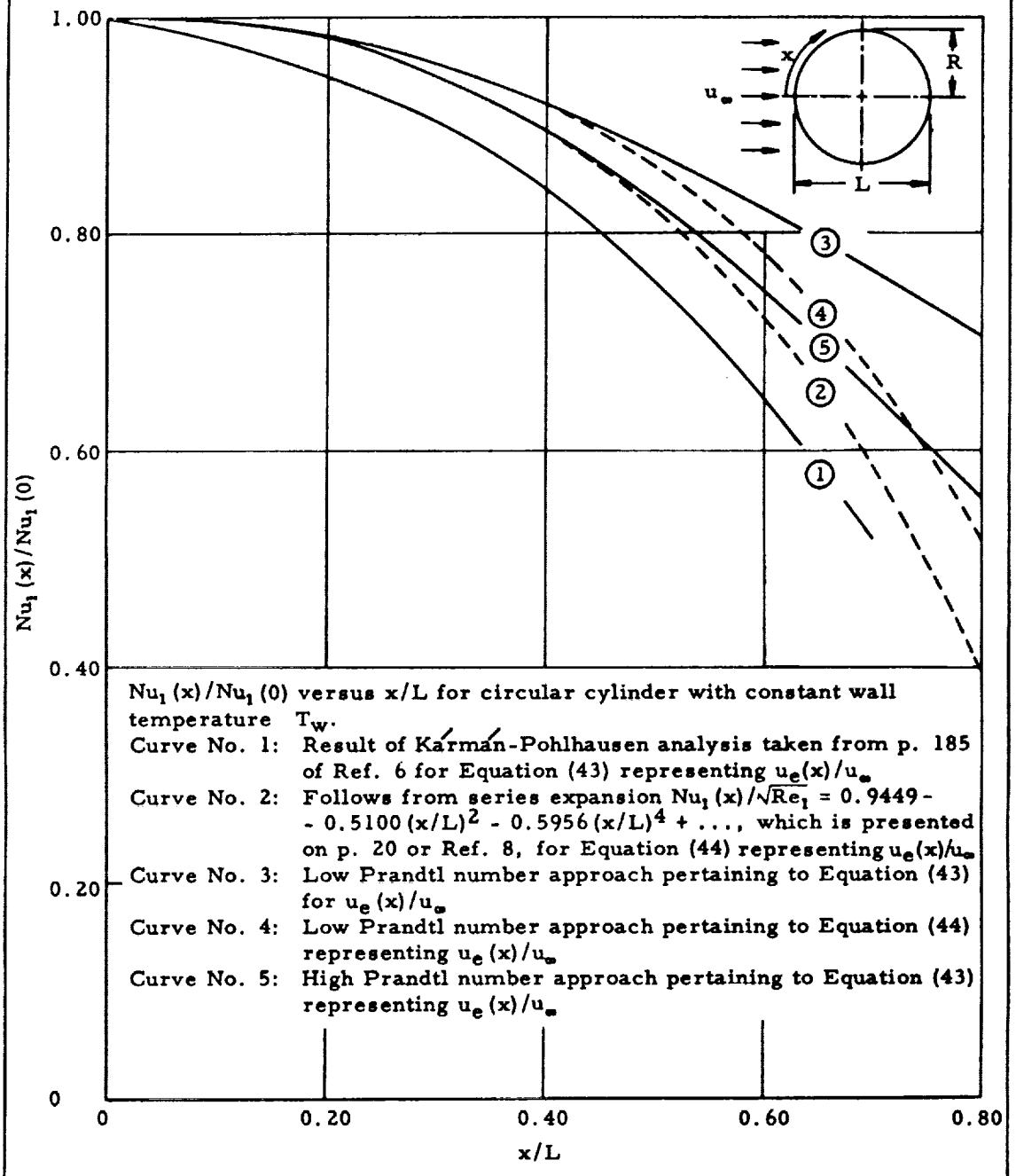

$Nu_1(x)/Nu_1(0)$ versus x/L for circular cylinder with constant wall temperature T_W.

Curve No. 1: Result of Kármán-Pohlhausen analysis taken from p. 185 of Ref. 6 for Equation (43) representing $u_e(x)/u_\infty$

Curve No. 2: Follows from series expansion $Nu_1(x)/\sqrt{Re_1} = 0.9449 - 0.5100\,(x/L)^2 - 0.5956\,(x/L)^4 + \ldots$, which is presented on p. 20 or Ref. 8, for Equation (44) representing $u_e(x)/u_\infty$

Curve No. 3: Low Prandtl number approach pertaining to Equation (43) for $u_e(x)/u_\infty$

Curve No. 4: Low Prandtl number approach pertaining to Equation (44) representing $u_e(x)/u_\infty$

Curve No. 5: High Prandtl number approach pertaining to Equation (43) representing $u_e(x)/u_\infty$

FIG. 13. $Nu_1(x)/Nu_1(0)$ FOR CIRCULAR CYLINDER, T_W = CONST.

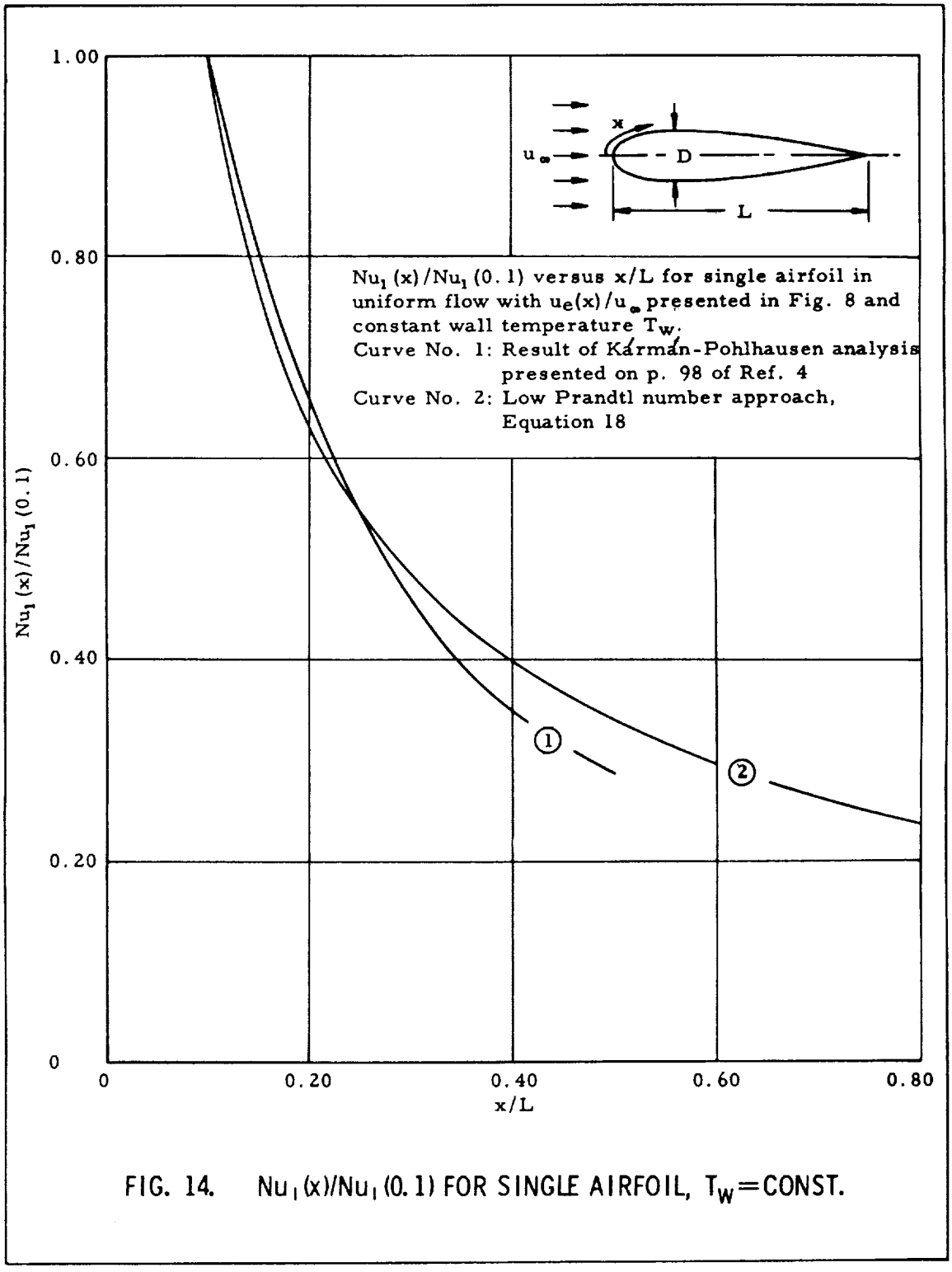

FIG. 14. $Nu_1(x)/Nu_1(0.1)$ FOR SINGLE AIRFOIL, T_W=CONST.

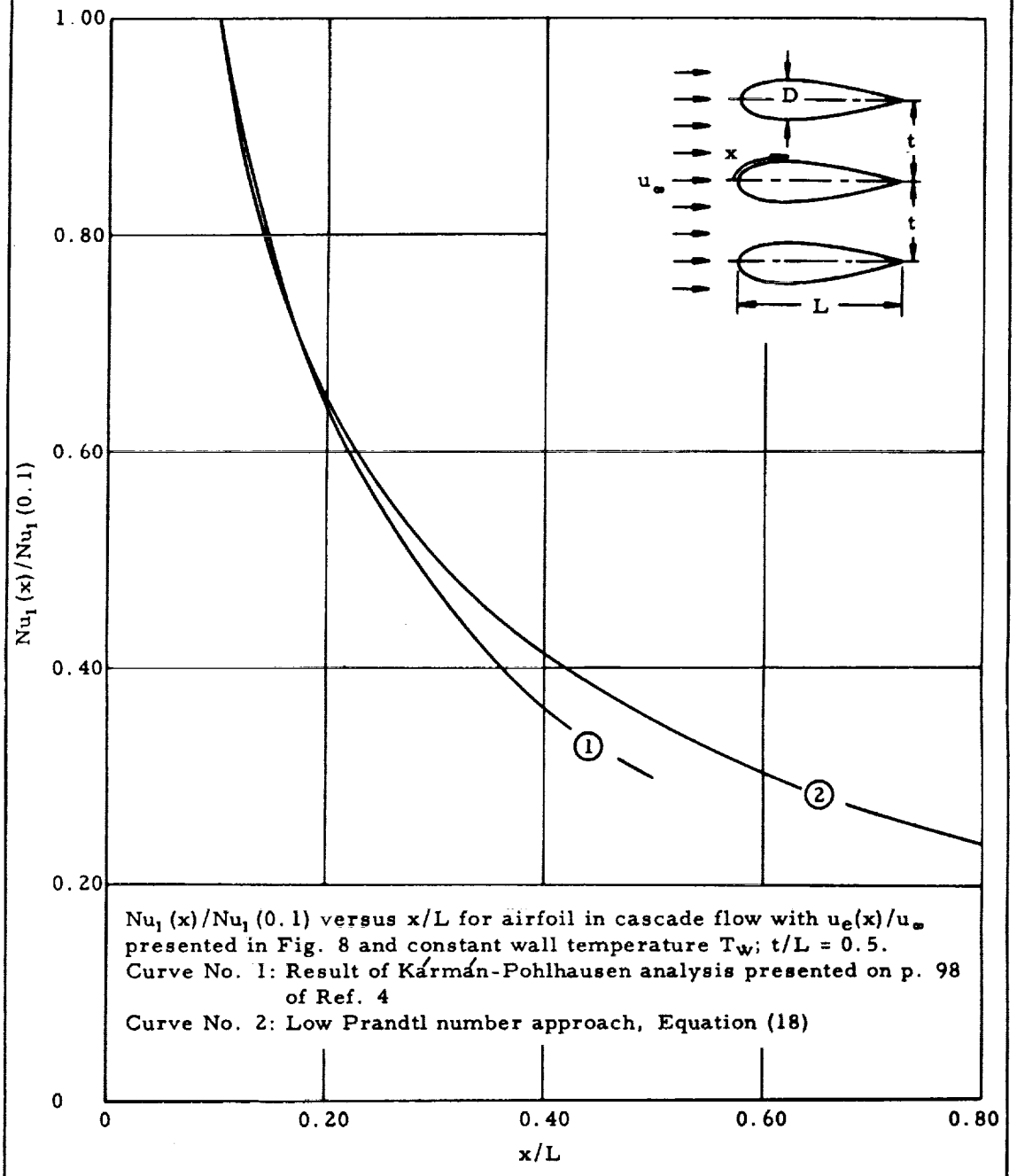

$Nu_1(x)/Nu_1(0.1)$ versus x/L for airfoil in cascade flow with $u_e(x)/u_\infty$ presented in Fig. 8 and constant wall temperature T_W; t/L = 0.5.
Curve No. 1: Result of Kármán-Pohlhausen analysis presented on p. 98 of Ref. 4
Curve No. 2: Low Prandtl number approach, Equation (18)

FIG. 15. $Nu_1(x)/Nu_1(0.1)$ FOR AIRFOIL IN CASCADE, T_W = CONST.

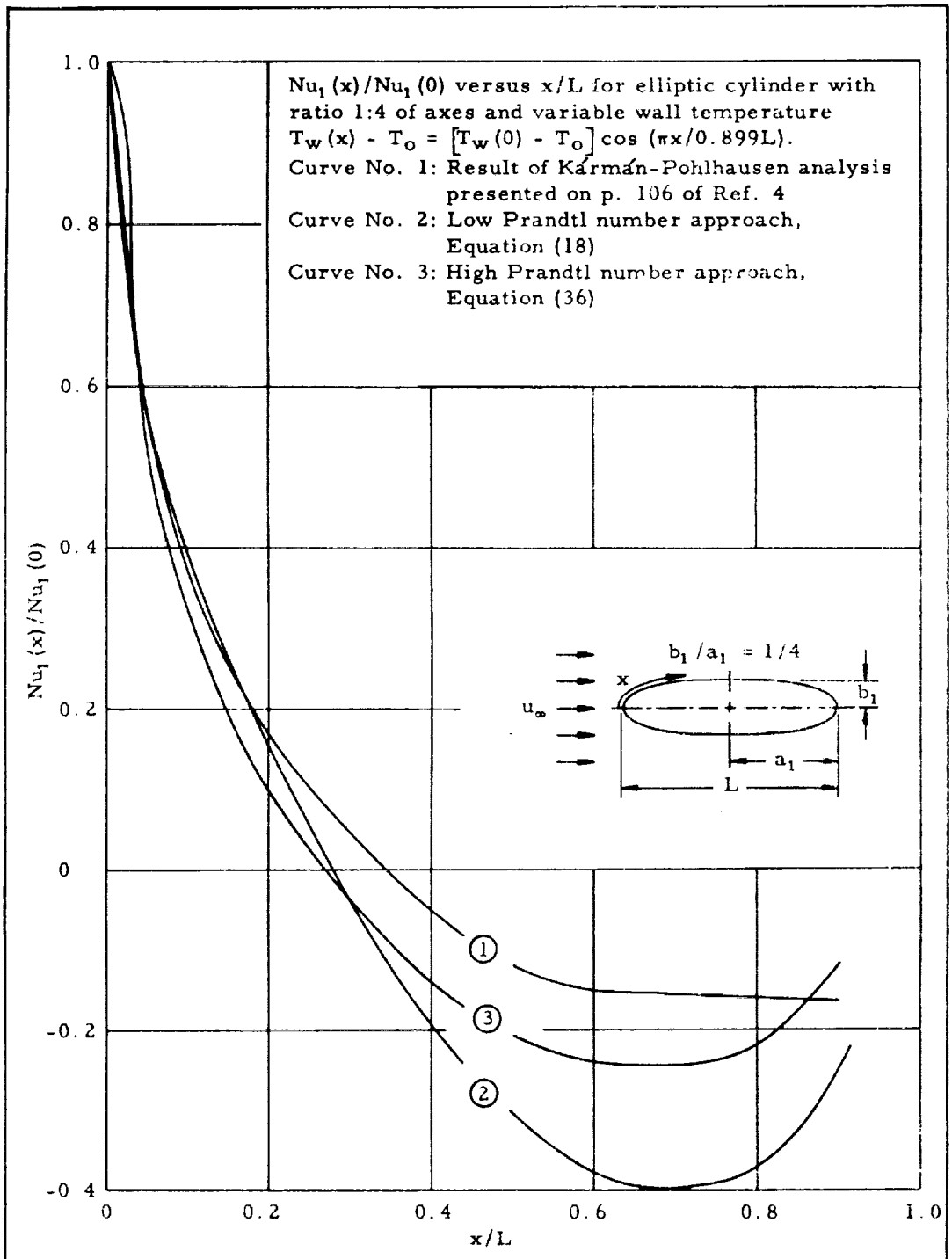

FIG. 16. $Nu_1(x)/Nu_1(0)$ FOR ELLIPTICAL CYLINDER 1:4, $T_W \neq$ CONST.

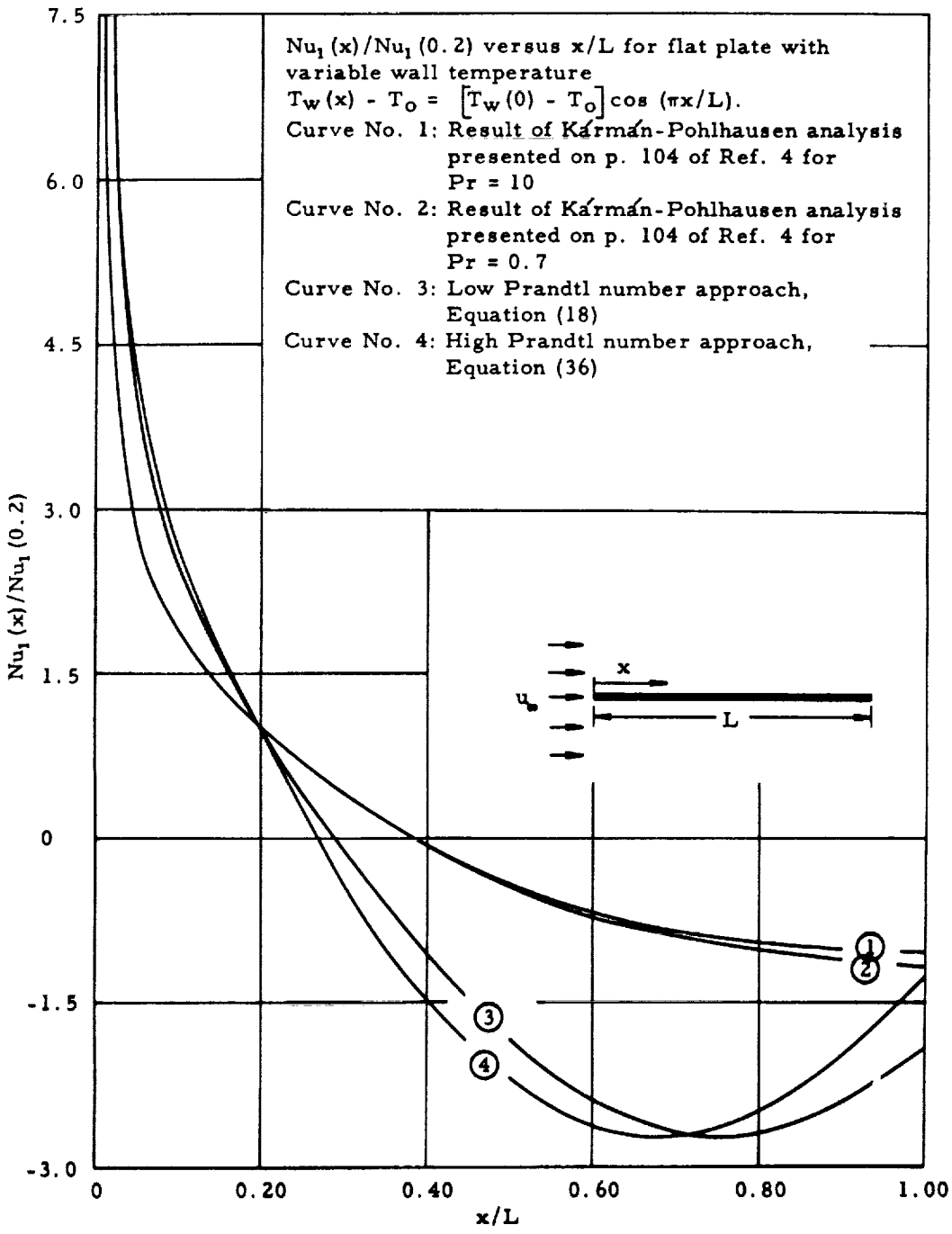

FIG. 17. $Nu_1(x)/Nu_1(0.2)$ FOR FLAT PLATE, $T_W \neq$ CONST.

$Nu_3(x)/Nu_3(0)$ versus x/L for flat plate with variable wall temperature $T_w(x)/T_o = 1.25 - 0.83x/L + 0.33(x/L)^2$, where $Nu_3(x) = xq_w(x)/kT_o$.
Curve No. 1: Result of exact series expansion of solution on p. 561 of Ref. 2
Curve No. 2: Low Prandtl number approach, Equation (12)
Curve No. 3: High Prandtl number approach, Equation (32)

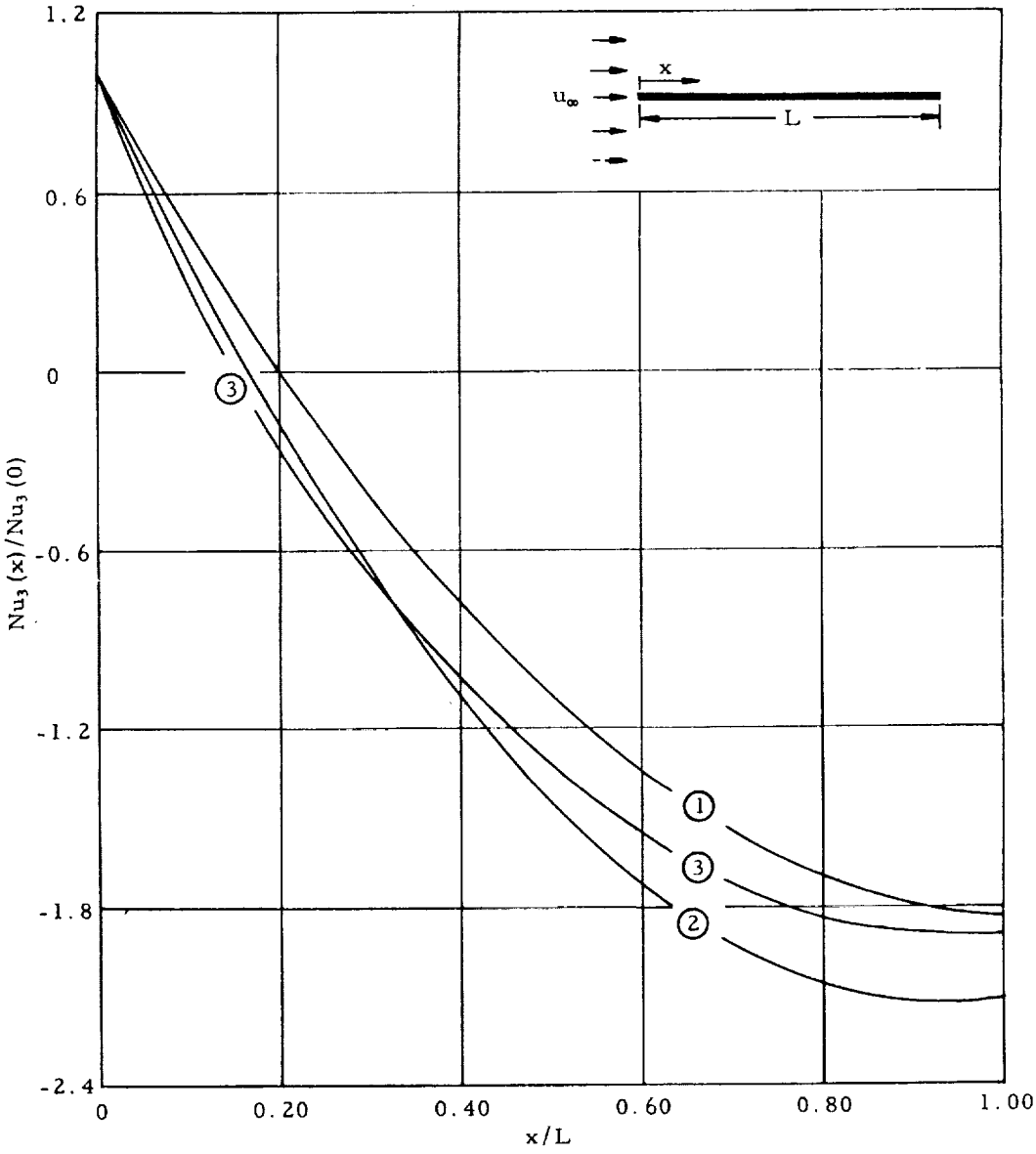

FIG. 18. $Nu_3(x)/Nu_3(0)$ FOR FLAT PLATE, $T_w \neq$ CONST.

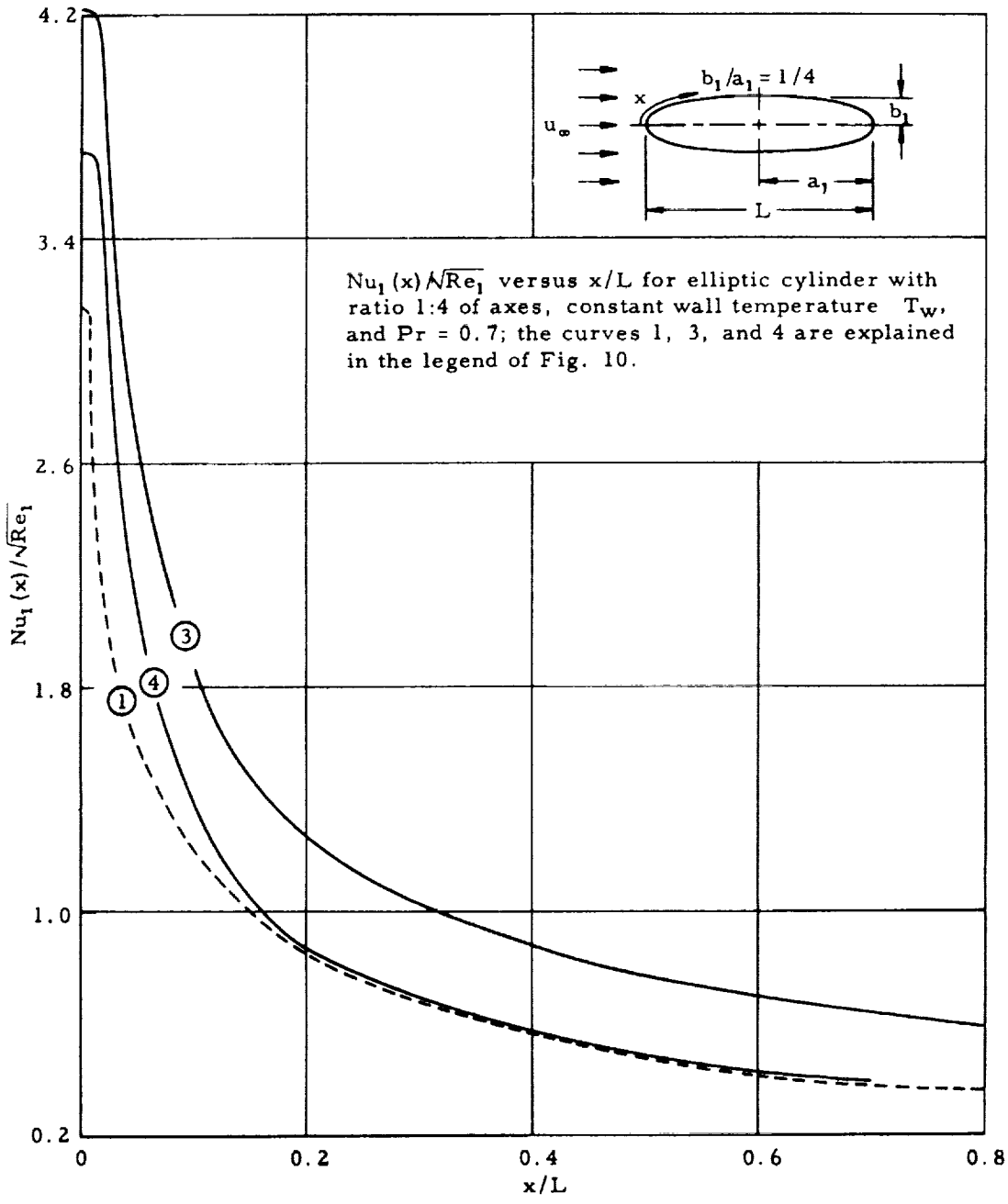

FIG. 19. $Nu_1(x)/\sqrt{Re_1}$ FOR ELLIPTICAL CYLINDER 1:4, T_W = CONST.

$Nu_1(x)/\sqrt{Re_1}$ versus x/L for circular cylinder with constant wall temperature T_w, and Pr = 0.7; the curves 1, 3, and 5 are explained in the legend of Fig. 13.

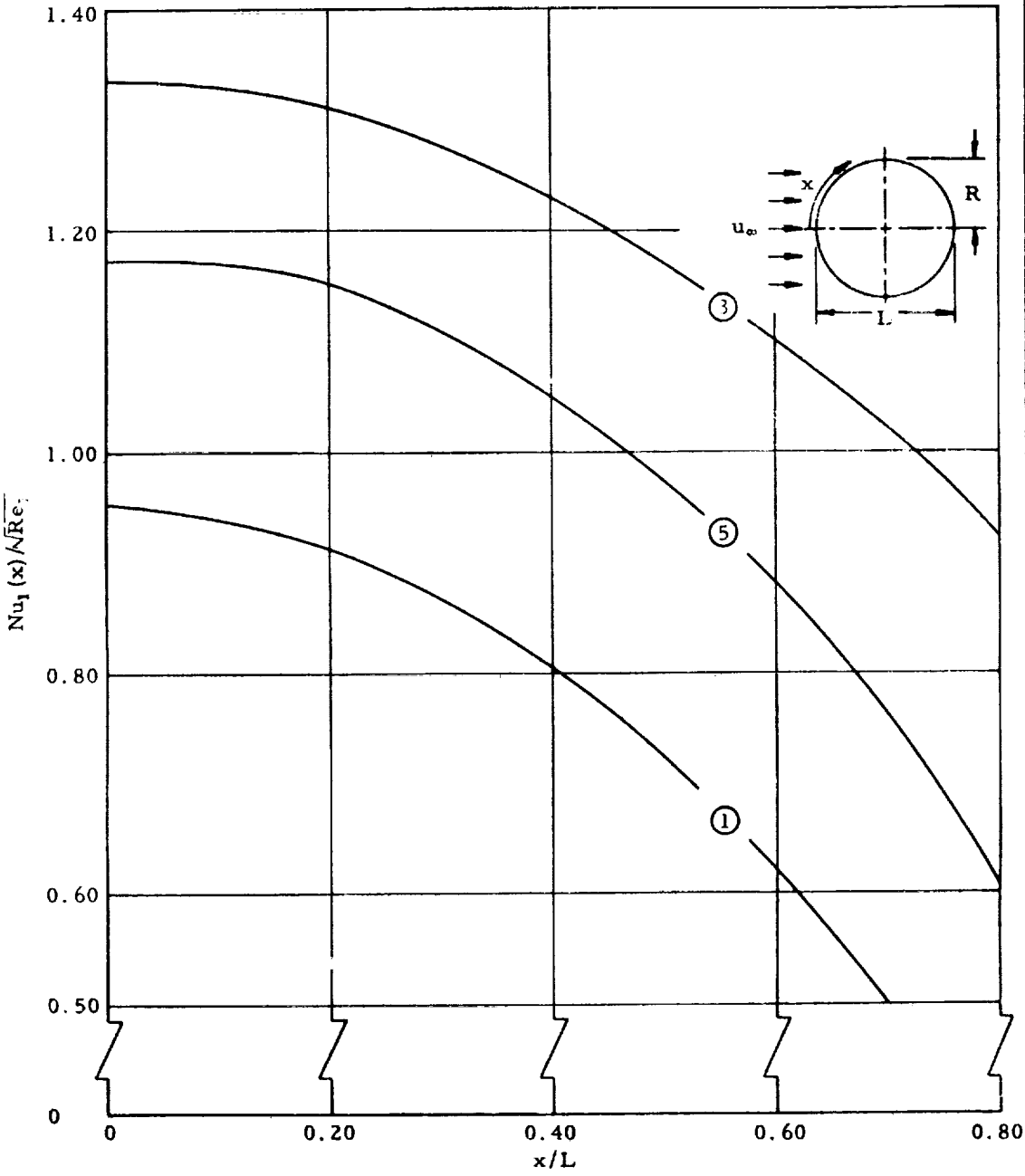

FIG. 20. $Nu_1(x)/\sqrt{Re_1}$ FOR CIRCULAR CYLINDER, T_W=CONST.

REFERENCES

1. Carslaw, H. S., and J. C. Jaeger, Conduction of Heat in Solids, Oxford University Press, Second Edition, London, 1959.

2. Chapman, D. R., and M. W. Rubesin, Temperature and Velocity Profiles in the Compressible Laminar Boundary Layer with Arbitrary Distribution of Surface Temperature, J.Ae.Sc., vol. 16, 1949, p. 547.

3. Curle, N., Heat Transfer Through a Constant Property Laminar Boundary Layer, A.R.C., 22,584, F.M.3054, Feb. 1961.

4. Dienemann, W., Berechnung des Wärmeüberganges an laminar umströmten Körpern mit konstanter und ortsveränderlicher Wandtemperatur, ZAMM, vol. 33, 1953, p. 89.

5. Donoughe, P. L., and J. N. B. Livingood, Exact Solutions of Laminar-Boundary Layer Equations with Constant Property Values for Porous Wall with Variable Wall Temperature, NACA Tech. Rep. TR 1229, Washington, 1955.

6. Eckert, E. R. G., and R. M. Drake, Jr., Heat and Mass Transfer, McGraw-Hill Book Co., New York, 1959.

7. Frank, P., and R. v. Mises, Die Differentialgleichungen und Integralgleichungen der Mechanik und Physik, vol. 2, Second Edition Dover Publications, New York, 1961.

8. Frössling, N., Evaporation, Heat Transfer, and Velocity Distribution in Two-Dimensional and Rotationally Symmetrical Laminar Boundary-Layer Flow, NACA Tech. Memo. TM 1432, Washington, Feb. 1958.

9. Hartree, D. R., On an Equation Occurring in Falkner and Skan's Approximate Treatment of the Equations of the Boundary Layer, Proc. Cambr. Phil Soc., vol. 33, part II, 1937, p. 223.

10. Levy, S., Heat Transfer to Constant-Property Laminar Boundary-Layer Flows With Power-Function Free-Stream Velocity and Wall-Temperature Variation, J.Ae.Sc., vol. 19, 1952, p. 341.

11. Liepman, H. W., A Simple Derivation of Lighthill's Heat Transfer Formula, J. Fluid Mechanics, vol. 3, 1958, p. 357.

12. Lighthill, M. J., Contributions to the Theory of Heat Transfer Through a Laminar Boundary Layer, Proc.Roy.Soc., A, vol. 202, 1950, p. 359.

REFERENCES (CONT'D)

13. Millsaps, K., and K. Pohlhausen, Thermal Distribution in Jeffery-Hamel Flows Between Non-Parallel Plane Walls, J.Ae.Sc., vol. 20, 1953, p. 187.

14. Morgan, G. W., A. C. Pipkin, and W. H. Warner, On Heat Transfer in Laminar Boundary Layer Flows of Liquids Having a Very Small Prandtl Number, J.Ae.Sc., vol. 25, 1958, p. 173.

15. Pai, S., Viscous Flow Theory, Part I, D. Van Nostrand Co., Princeton, 1956.

16. Pohlhausen, K., Der Wärmeubergang zwischen festen Körpern und Flüssigkeiten mit kleiner Reibung und kleiner Wärmeleitung, ZAMM, vol. 1, 1921, p. 115.

17. Schlichting, H., Der warmeübergang an einer längsangeströmten ebenen Platte mit veränderlicher Wandtemperatur, Forsch. Ingenieurwesen vol. 17, 1951, p. 1.

18. Schlichting, H., and E. Truckenbrodt, Aerodynamik des Flugzeuges, Springer, Berlin, 1959.

19. Schlichting, H., Boundary Layer Theory, Pergamon Press, London, 1955.

20. Spalding, D. B., Heat Transfer From Surfaces of Non-Uniform Temperature, J. Fluid Mechanics, vol. 4, 1958, p. 22.

21. Sparrow, E. M., Analysis of Laminar Forced-Convection Heat Transfer in Entrance Region of Flat Rectangular Ducts, NACA Tech Note TN 3331, 1955.

22. Sparrow, E. M., and J. L. Gregg, Details of Exact Low Prandtl Number Boundary Layer Solutions for Forced and for Free Convection, NASA Memo 2-27-59-E, Washington, 1959.

23. Squire, H. B., Heat Transfer Calculations for Aerofoils, ARC R&M 1986, 1942.

NASA-Langley, 1963 D-1527